Received: 28 February 2022 | Revised: 20 March 2022 | Accepted: 23 March 2022

DOI: 10.1002/bio.4242

LUMINESCENCE WILEY
The Journal of Biological and Chemical Luminescence

REVIEW

Technological advancements in bio-recognition using liquid crystals: Techniques, applications, and performance

Rajesh[1,2] | Lokesh K. Gangwar[1,2] | Sujeet K. Mishra[3] | Amit Choudhary[4] | Ashok M. Biradar[1,2] | Gajjala Sumana[1,2]

[1]CSIR-National Physical Laboratory, New Delhi, India

[2]Academy of Scientific and Innovative Research (AcSIR), Gaziabad, India

[3]Central Ayurveda Research Institute, Jhansi, India

[4]Physics Department, Deshbandhu College (University of Delhi), New Delhi, India

Correspondence
Rajesh, CSIR-National Physical Laboratory, Dr K. S. Krishnan Marg, New Delhi 110012, India.
Email: rajesh_csir@yahoo.com

Funding information
Council of Scientific and Industrial Research, India; National Physical Laboratory

Abstract

The application of liquid crystal (LC) materials has undergone a modern-day renaissance from its classical use in electronics industry as display devices to new-fangled techniques for optically detecting biological and chemical analytes. This review article deals with the emergence of LC materials as invaluable material for their use as label-free sensing elements in the development of optical, electro-optical and electrochemical biosensors. The property of LC molecules to change their orientation on perturbation by any external stimuli or on interaction with bioanalytes or chemical species has been utilized by many researches for the fabrication of high sensitive LC-biosensors. In this review article we categorized LC-biosensor based on biomolecular reaction mechanism viz. enzymatic, nucleotides and immunoreaction in conjunction with operating principle at different LC interface namely LC-solid, LC-aqueous and LC-droplets. Based on bimolecular reaction mechanism, the application of LC has been delineated with recent progress made in designing of LC-interface for the detection of bio and chemical analytes of proteins, virus, bacteria, clinically relevant compounds, heavy metal ions and environmental pollutants. The review briefly describes the experimental set-ups, sensitivity, specificity, limit of detection and linear range of various viable and conspicuous LC-based biosensor platforms with associated advantages and disadvantages therein.

KEYWORDS
biosensor, DNA, liquid crystals, proteins, thermotropic

1 | INTRODUCTION

Liquid crystals (LCs) are smart and soft materials and they have been utilized in various technological innovations and applications such as LC displays, sensors, solar cells and modulators, etc. The scientific and technological revolution that these materials have brought in the field of high resolution displays have ushered in a new age in technological advancement.[1] Various other technologically advanced LC-based materials include colour changing clothes, eyewear switching from light to dark, smart glasses to control the amount of heat and light passing through them and many more.[2] However, the concept of LC phase is not limited to classical systems but the same has been taken to quantum mechanics in two and three dimensions by considering the spin of electrons in metals.[3,4] The paradigm of LC research has now been shifted towards the field of bioscience from where its knowledge was first originated in cholesteryl benzoate.[5] LC phase comprising of agglomeration of non-spherical molecules in mesophase manner resulted from the partial deviation of perfect positional and orientational order of the crystal lattice and acquiring fluidic behaviour of liquids.[6–9] They have been widely explored for the purpose of biosensing application but still not to the high end biosensing so that the final technology could be realized in the market. Though recently a few review articles have been reported,[10–12] this article is focused on the application of LCs based on biomolecular reaction mechanism

viz enzyme-analyte interactions, nucleic acid hybridization and immunoresponse occurring at different LC-interface along with the role of nanoscale dopants and cationic surfactants for proteins, virus, bacteria, clinically relevant compounds, heavy metal ions and environmental pollutants detection.

1.1 | Types of liquid crystals for biosensing

All the LC phases of material are not suitable for the biosensing purposes due to the fact that the force of interaction responsible for balancing the molecules in LC phase could not induce the bio-interfacial perturbing signals for the detection. However, in general, there are two generic classes of LCs (i) thermotropic LCs, whose molecular orientation in LC phase is temperature dependent which is lost after certain temperature, called as transition temperature of LC to isotropic phase and (ii) lyotropic LCs, whose molecular orientation in LC phase is influenced by solvents and LC phase is lost after certain concentration of solvent. Thermotropic LCs exhibit high degree of shape anisotropy with either rod like or disc like molecules.[13–17] Rod like molecules are further classified into nematic LC when the bulk system possesses orientational order but lacks positional order while if positional order is also maintained along with the orientational ordering, the phase is known as smectic phase. These phases are further distinguished by the general direction of orientation of the axes of the molecules along the director '*n*'. When each layer of nematic LC is faintly twisted relative to the next leading to the generation of a helix perpendicular to the molecular axis, then it is known as twisted or cholesteric nematic LC. The most widely exploited LC phase in biosensing is nematic phase due to its easier perturbation of molecular alignment at the interface of biomolecules and LC which is marked as sensing tool if observed optically.

1.2 | Principle of biosensing using LC

The use of LCs in sensing application is attributed to their unique rapid optical responsiveness to any external stimuli. The adsorption of any surface-active molecules such as surfactants, lipids[18–22] or non-surface-active molecules such as gas vapours[23–26] or specific biomolecules[15,27–29] on the surface of LC can disrupt the inherent alignment of the mesophase at the interface, which propagates into the bulk LC up to 1 mm in depth.[29] As a result of which a small perturbation caused by a few molecules at the surface is amplified to striking optical effects (change in colour from black to white) that can be easily seen without the use of any fluorescent dyes. The mechanism of optical sensing is based on the generation of director defect when the size of the substance in the medium of LCs is larger than '*b*', the extrapolation length as given by the following equation[30,31]:

$$b = \frac{K}{W} \quad (1)$$

where W is anchoring strength between the object and the liquid crystal medium with values in the range of 10^{-3} to 10^{-5} J m^{-2} and K is the director curvature elastic constant having values ranging from 1 to 10 pN. The size of the biomolecule becomes larger after binding with its complementary molecule (as in the case of antibody–antigen complex formation during immunoreaction) which results in the disruption of liquid crystalline alignment, thereby altering the birefringence profile and optical texture is visualized using polarized optical microscopy (POM).[32–38] The sensitivity of the LCs towards the surface in contact with it is due to the fine balance between the surface anchoring energy of the director '*n*' and bulk elastic deformation of LC molecules. The nature and extent of alterations induced in the orientation of director of the aligned LC by the desired target upon coming in contact with it depends on the structure of the modifying material[39–42] and the type of process occurring at the LC interface (LC-solid, LC-aqueous or LC-droplets)[43–52] that disrupts or perturbs the LC orientation. The light that is passed through the optically anisotropic molecules of LC gets modulated resulting in the generation of an optical signal.

In liquid–solid interface sensing, LC cells are constructed with assembled monolayer of silane like DMOP (dimethyl octadecyl (3-[trimethoxysilane] propyl) ammonium chloride) coated cover and bottom microscopic glass slides which induces vertical alignment of LCs separated by a Mylar polyester film spacer having an inlet on one side with binding/adhesion and a drop of 4-cyano-4′-pentyl biphenyl (5CB) is drawn inside the cell through capillary effect. The surfaces of these silylated microscopic glass slides are modified with either ligands for protein detection or bio/chemical receptors for bio/chemical detection which does not change the vertical alignment of 5CB showing a featureless image but are perturbed on interaction with target molecule upon enzymatic, antibody–antigen or hybridization/coordination interactions, inducing brightness of the LCs viewed under the cross polarizers.[41] However, to understand the interfacial phenomena in real time, LC-liquid interface was found to be a suitable sensing system as biomolecular interactions are mostly occurring in aqueous solution wherein a biomolecule retains both its structural and functional activity. In LC-liquid interface biosensor, a transmission electron microscopy (TEM) copper or gold grid is placed over a silylated microscopic glass slide that provides a homeotropic alignment of LCs showing an all-black image, which upon immersing into an aqueous phase in conjunction with a biomolecular interaction with the target analyte taking place at the interface produces a planer alignment, showing an optical image back from black to bright image, under the cross polarizers. The use of LC as optical sensing elements for the detection of biomolecules is credited to Abbott and co-workers[53] who have extensively studied the effect of biomolecules and other molecules like polymer electrolyte,[54] ionic surfactants[39] and amphiphilic molecules[55] on the orientation of liquid crystalline arrangement at LC-aqueous interface. Apart from LC-aqueous interface sensing, another sensing mechanism comprising LC-droplet interface has also been extensively studied wherein the LCs are emulsified to LC droplets by using mini-emulsion technique[40] or polymer shells as template,[43] and microfluidic approach etc.[45,46] These LC droplets

which have initially a bipolar configuration get changed into a radial configuration upon interacting with amphiphilic molecules hence provide a sensing response in detecting various biomolecules[47,48] including bacteria and viruses.[49] A detailed description of the biosensing mechanism with different LC-interfaces has been delineated according to the type of biomolecules used and their applications in various fields under sections given later.

2 | TYPES OF LC BIOSENSORS BASED ON BIOMOLECULES

Biosensors are analytical devices and are being used for a number of applications such as clinical diagnostics, chemical detection, heavy metal detection, quality of food, water, beverages, and defence related applications. The mechanism of biosensing is the adoption of specific biological components such as micro-organisms, clinically relevant compounds, tissues, whole cells, cell receptors, enzymes,[56] antibodies[57,58] and nucleic acids,[59] etc. for the detection of various analytes using a suitable transduction mechanism having optical,[28] thermal, electrochemical[60] or field-effect transistor techniques.[61] Contrary to the conventional techniques for biomolecular detection such as ELISA,, optical assays, Phage and ribosome display, etc.[62,63] LC-based sensing technique is label-free, portable, cost-effective, requires lesser detection time and does not require any sophisticated equipment and hence has the potential to replace the traditional sensing techniques. In recent past, LCs have been explored for various biosensor applications using various biocomponents such as enzymes, proteins/antibodies and nucleic acids/aptamers. We categorized these LC-based biosensors according to the type of biomolecules used as schematically presented in Figure 1 and briefly described the biomolecular reaction mechanisms along with the working principle involved therein. The sensing performance of various LC biosensor devices for biological and chemical analytes is summarized in Table 1.

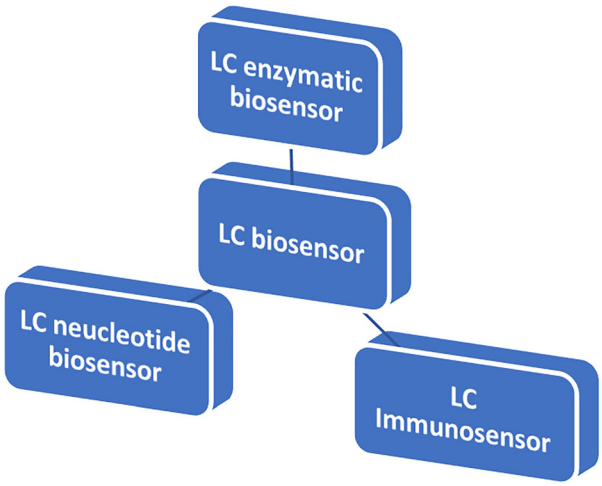

FIGURE 1 Schematic presentation of type of liquid crystal biosensors

2.1 | LC enzymatic biosensors

An enzymatic biosensor is an analytical device which is based on the specific enzyme-analyte interaction coupled with a suitable transducer to generate a quantifiable response with respect to target analyte concentration. The suitable transducer system such as electrochemical, optical or thermal transduction converts the enzymatic reaction into a measurable signal such as current, voltage, temperature change, or colour, flouroscence intensity, etc. In LC-enzymatic sensors, orientational changes and dielectric properties in LCs with respect to enzyme-analyte binding is studied and are reported to be highly sensitive. Kim et al.[45] used small micro-meter sized 5CB LC droplets generated using microfluidic technique for the detection of glucose in aqueous medium. For the formation of LC droplets a continuous phase comprising of poly(acrylic acid-4-cyano biphenyl-4-oxy undecyl acrylate) and dispersed phase of 5CB were injected in the microfluidic channels. Glucose oxidase (GO_x) enzyme was covalently immobilized on $5CB_{PAA}$ LC droplets and then utilized as pH-sensitive glucose biosensor. A small change in pH due to enzymatically produced H^+ ions when glucose gets converted to gluconic acid in the presence of GO_x enzyme (Equation 2) causes orientational alteration of LC droplets from radial configuration to bipolar configuration.

$$\text{Glucose} \xrightarrow{\text{Glucose oxidase}} \text{Gluconate ion} + H^+ \quad (2)$$

This technique has been able to detect glucose of very low concentration upto 0.03 mM at a response time of 3 min. Further the specificity of the biosensor was tested by using another isomeric monosaccharide, galactose, which did not make any change in the initial radial orientation of LC droplets. Hoogboom et al.[99] utilized a water-soluble enzyme, lipase to catalyse the hydrolysis of ester contained group incorporated in the aligned self-assembled layer of liquid crystal cells. The partial hydrolysis of the siloxane layer containing hydrolysable ester group created a local disturbance in the alignment of 5CB nematic LC which was visualized using a polarized microscope. Upon hydrolysis, the interaction between LC molecules and the alignment layer changes from non-polar (between a polar part of 5CB and benzyl group) to polar (between polar part of 5CB and an acid group) interfacing forcing orientational change of mesogens LC near the boundary of enzymatic activity (Figure 2).

The polarizing microscope showed that areas of approximately 100 μm were disrupted on enzymatic activity. The method presented in this article can be used for detection of a class of enzymes but further investigations are required for the determination of lower limit of enzyme concentration that can be detected using such systems in relation to reaction time.

2.2 | LC nucleotide biosensor

LC nucleotide biosensors such as DNA hybridization biosensing systems have been developed in recent past in various fields, such as

TABLE 1 The sensing performance of various liquid crystal (LC) biosensor devices for biological and chemical analytes

LC used	LC-interface	Receptor (bio/chemical)	Analyte (bio/chemical)	Detection range	Limit of detection	Detection method	Ref.
Nematic 5CB	LC-aqueous	Avidin	Anti-Av-IgG	—	2.3 nM	POM	[28]
Nematic 5CB	LC-solid	Biotin	Anti-biotin IgG	1–100 nM	—	POM	[53]
E7 (mixture of cyanobiphenyls and a cyano terphenyl)	LC-aqueous	ssDNA	ssDNA complement	50–500 fmol	~50 fmol	Polarized and fluorescence microscopy	[64]
Nematic 5CB	LC-solid	DNA microarray	DNA	25–0.01 μM	0.5 μM	POM	[65]
Nematic 5CB	LC-solid	DNA	DNA	40-4 μg ml^{-1}	4 μg ml^{-1}	POM	[66]
Nematic 5CB	LC-aqueous	Peptide nucleic acid	DNA	-	10 fM	POM	[67]
Nematic 5CB	LC-aqueous	DNA functionalized Au-NPs	DNA	0.1–10 pM	0.1 pM	POM	[68]
Nematic 5CB	LC-droplet	ssDNA/dsDNA	ssDNA/dsDNA complement	0.2–30 μM	50 nM	POM and epi-fluorescence microscopy	[69]
Nematic 5CB	LC-solid	IgG	Anti-IgG	0.02–0.08 mg ml^{-1}	0.02 mg ml^{-1}	POM	[70]
Br-Py	LC-aqueous	Ab-myoglobin	Myoglobin	9.96–72.8 ng ml^{-1}	6.29 ng ml^{-1}	Electrochemical	[71]
Nematic 5CB	LC-droplet	Goat anti-IgG molecules	Rabbit IgG	20 to 1000 ng ml^{-1}	16 ng ml^{-1}	POM	[72]
Nematic 5CB	LC-aqueous	EGFR	Anti-phosphotyrosine IgG antibodies	10 pM to 100 nM	0.01 nM	Ellipsometry and POM	[73]
Twisted Nematic 5CB	LC-solid	EG4N	EGFR	30–40 pg mm^{-2}	0.3 fg	POM	[74]
Nematic 5CB	LC-solid	AuNPs/silane	BSA	0.5 to 100 μg ml^{-1}	0.5 μg ml^{-1}	POM	[75]
Eutectic- Nematic mixture	LC-solid	DMOAP	BSA	10^{-9} to 10^{-3} g ml^{-1}	15 pM	POM	[76]
Azobenzene based LC	LC-aqueous	DMOAP	BSA	1 to 7.5 μg ml^{-1}	—	electro-optical	[77]
Dual frequency LC	LC-solid	DMOAP	BSA	10^{-7} to 10^{-2} g ml^{-1}	10^{-7}	dielectric and POM	[78]
Polymer stabilized cholesteric LC	LC-aqueous	CLC	BSA	1 ng ml^{-1} to 2 mg ml^{-1}	1 ng ml^{-1}	Smartphone (optical)	[79]
Nematic 5CB	LC-aqueous	Antigen HBD-2	HBD-2	1–10 ng ml^{-1}	0.53 ng ml^{-1}	POM	[80]
Nematic 5CB	LC-aqueous	ChO_x	Cholesterol	10 to 250 mg dl^{-1}	-	POM	[81]
Nematic 5CB	LC-aqueous	AChE	AChE inhibitor neostigmine	1 μM to 10 pM	1 fM	POM	[82]
Thermotropic (E7)	LC-aqueous	ssDNA	SARS-CoV-2 ssRNA	30 fM to 100 nM	30 fM	POM	[83]
Nematic 5CB	LC-aqueous	Aptamer	Amoxicillin	1 μM to 5 nM	3.5 nM	POM	[84]
Nematic 5CB	LC-aqueous	Anti-cTnI	cTnI	0.0001 ng ml^{-1} to 1000 ng ml^{-1}	1 pg ml^{-1}	POM	[85]

TABLE 1 (Continued)

LC used	LC-interface	Receptor (bio/chemical)	Analyte (bio/chemical)	Detection range	Limit of detection	Detection method	Ref.
Nematic 5CB	LC-droplet	Urease	Urea	—	3 mM	POM	[40]
Nematic 5CB	LC-droplet	GO_x Enzymes	Glucose	—	0.03 mM	POM	[45]
Nematic 5CB	LC-droplet	Bacteria (Gram-positive and Gram-negative) and viruses (enveloped and non-enveloped)	Virus and bacteria	1–5 (*E. coli*)	10^4 pfu ml^{-1} (Influenza A)	POM	[49]
Nematic 5CB	LC-aqueous	DNA aptamer	Hg^{2+}	0.1 to 5 nM	0.1 nM	POM	[86]
Nematic 5CB	LC-aqueous	*N*-Methyl-*N*-dodecyldithiocarbamate	Hg^{2+}	0.5 μM to 200 μM	0.5 μM in deionized water sample and 10 μM in tap water	POM	[87]
Nematic 5CB	LC-droplet	Aptamer	Hg^{2+}	50 to 500 pM	100 pM	POM	[88]
Nematic 5CB	LC-aqueous	SRNA	Pb^{2+}	3 to 75 nM	3 nM	POM	[89]
Nematic 5CB	LC-aqueous	Ars-3 aptamer	As^{3+}	0.02 to1 μM	50 nM	POM	[90]
Nematic 5CB	LC-aqueous	DNA strand	Pb^{2+}	20 nM to 100 μM	0.65 nM	fluorescence and optical	[91]
Nematic 5CB	LC-droplet	AChE	Baycarb and dimethoate	0.1 ng ml^{-1} to 1 μg ml^{-1}	0.01 pg and 0.1 pg	POM	[92]
Nematic 5CB	LC-aqueous	AChE	Dimethoate	0.5 ng ml^{-1} to 8 ng ml^{-1}	0.9 ng ml^{-1}	POM	[93]
Nematic 5CB	LC-droplet	AChE	Fenobucarb and malathion	—	5 pg ml^{-1} (fenobucarb) and 2.5 pg ml^{-1} (malathion)	POM	[94]
Nematic 5CB	LC-aqueous	Aptamer	Malathion	0.8 to 50 pM	2.5 pM	POM	[95]
Nematic 5CB	LC-droplet	Alkaline phosphatase	Dichlorvos pesticide	0.01 ng ml^{-1} to 1 μg ml^{-1}	0.1 ng ml^{-1}	POM	[96]
Nematic 5CB	LC-aqueous	Aptamer	Bisphenol A	0.60 to 20 nM	600 pM	POM	[97]
Nematic 5CB	LC-aqueous	aptamer	PCB77	5×10^{-5} to 5×10^{1} nM.	1.5×10^{-5} μg L^{-1}	POM	[98]

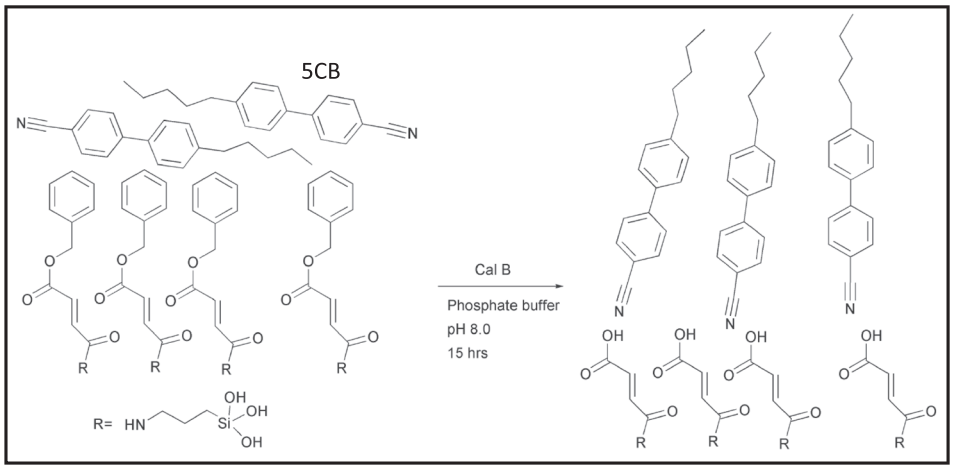

FIGURE 2 Schematic depiction of possible extreme differences in local liquid crystal orientation, arising from polarity differences upon hydrolysis of the alignment layer, resulting in a reorientation of the mesogen near the boundary of enzymatic action and interfering with uniform liquid crystal alignment (adapted from Hoogboom et al.[99] with permission from Royal Society of Chemistry)

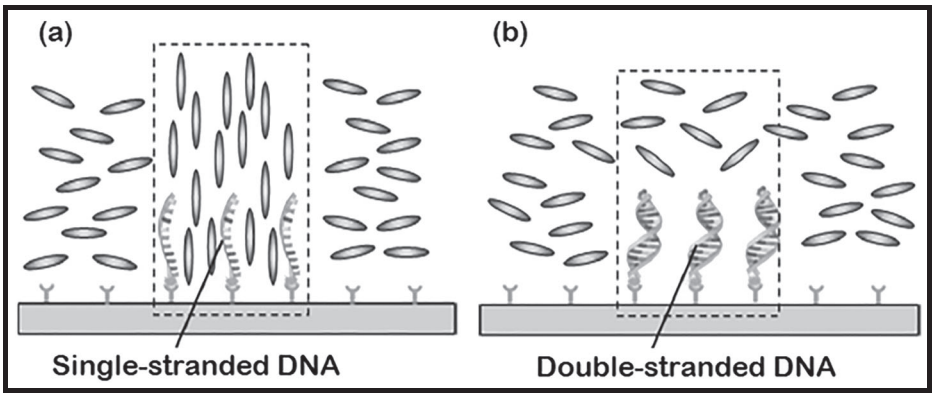

FIGURE 3 The nematic LC (5CB) alignment states under the two packing density conditions of the immobilized layer (a) before hybridization, the nematic LC molecules in the bulk are homoetropically aligned by a steric interaction between the freely penetrated nematic LC molecules and the single stranded DNA (ssDNA) immobilized normal to the substrate and subsequent propagated elastic interaction, (b) after hybridization, the penetration of the nematic LC molecules is hindered by the double stranded DNA (dsDNA) due to their increased packing density (adapted from Kim et al.[104] with permission from Institute of Physics)

clinical diagnostics,[100] gene analysis,[101] food safety[102] and agricultural industries,[103] etc. In nuceic acid-based sensor systems, it often requires amplification methods such as polymerase chain reaction (PCR) to achieve the desired quick response, sensitivity, and detection range, etc. However, the LC-based imaging system provides a simple tool for the detection of DNA hybridization without using any expensive detection equipment for various applications as LC orientation is quite sensitive towards any physical or chemical alterations occurring on the surface. Kim et al.[104] demonstrated the specific hybridization of single stranded DNA (ssDNA) having 19 oligonucleotide sequence with its complementary DNA sequence using a simple, cost-effective optical detection system utilizing orientation properties of nematic LC. Initially a homeotropic alignment of LC was obtained when ssDNA was immobilized on a Biotin chip pre-treated with calixarene derivative. The homeotropic alignment was achieved due to the steric interaction between the freely penetrated LC molecule and the surface immobilized ssDNA. But the orientation changed to planar inhomogeneous texture after the hybridization with the complementary DNA sequence. The formation of double stranded DNA (dsDNA) hindered the free penetration of LC molecules due to the increased packing density of dsDNA on the surface (Figure 3) and thus changing the orientation of LC which is then effectively transduced into optical signal by the crossed polarizer system.

Nakata et al.[105] and subsequently Malone et al.,[106] have investigated the alignment of achiral LC on aligned films of DNA on self-assembled monolayers of 3-glycidoxy propyl trimethoxy silane and octadecyl triethoxy silane. The authors have studied the influence of alignment of various non-chiral liquid crystals viz. nematic and smectic A liquid crystals on the surfaces of nucleic acid anchored self-assembled monolayers. The results indicated that distinctly chiral rotated structures have been obtained with a significant angle with respect to DNA orientation due to the dipolar and hydrophobic coupling. The key observations from both the research works are (i) LC got aligned in the direction of ssDNA extension whereas in the case of dsDNA, tilted angle alignment has been obtained (Figure 4) and (ii) very low density of DNA on the substrate surface can be imaged using LCs and hence sensitive DNA sensors can be framed using the orientation assumed by LCs in presence of DNA.

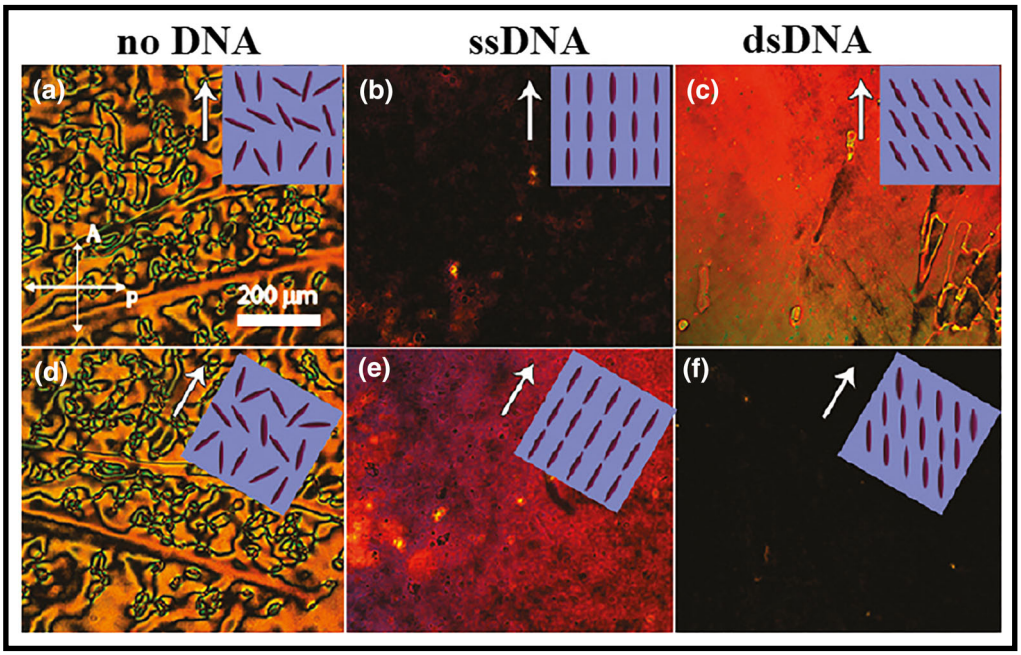

FIGURE 4 Polarized light images of hybrid aligned LC cells made with 3-glycidoxy propyl trimethoxy silane and octadecyl triethoxy silane. A dark image indicates LC alignment in the direction of polarizer or analyser. The insets show the alignment of LCs that is consistent with the respective images. (a) Control sample dipped in buffer with no DNA at 0° rotation (dipping direction aligned with the analyser). (b) ssDNA decorated surface at 0° rotation. (c) dsDNA decorated surface at 0° rotation. (d) Control sample dipped in buffer with no DNA at 30° rotation. (e) ssDNA decorated surface at 30° rotation. (f) dsDNA decorated surface at 30°, indicating LCs alignment at 30° (adapted from Malone et al.,[106] with permission from American Chemical Society)

Price and Schwartz[64] have investigated the interaction of DNA with octadecyl- trimethylammonium bromide (OTAB) surfactant adsorbed on LC, E7 in aqueous interface using fluorescence microscopy and POM. Results indicated that the OTAB adsorption on LC has induced a homeotropic alignment leading to appearance of dark textures when seen through a polarizing microscope. On subsequent addition of ssDNA to the OTAB loaded LC-aqueous interface, an electrostatic complex formation takes place between the surfactant having positive charge and negatively charged DNA, changing the orientation of LC to an intermediate tilt angle. It is further depicted that the formation of a duplex (hybridization) on addition of complementary ssDNA and thus breaking the DNA-surfactant complex. The label-free system has been found to detect very low concentration of 16 oligonucleotide sequenced DNA with a lower detection limit of 50 fM with a high selectivity. The LC-based DNA sensor has been found to differentiate even a mismatch of single base pair with respect to target complementary DNA sequence. However, the absence of a solid surface makes this method unsuitable for DNA microarray technology.

The nematic 5CB LCs were utilized by Lai et al.[65] to report the spatial distribution of oligonucleotides immobilized on DNA microarrays. The findings reported in this article can be used to pinpoint any defects present on the DNA microarray before the hybridization step. (Triethoxysilyl) butyl aldehyde (TEA)/*N*,*N*-dimethyl-n-octa decyl-3-amino propyltrimethoxy silyl chloride (DMOAP)-decorated surface was used as a microarray substrate to immobilize amine-labelled DNA sequence. The presence of thin layer 5CB LC on the substrate clearly differentiate between the absence (dark spot) and presence (bright spot) of oligonucleotides. Further the defects on the microarray after immobilization of oligonucleotides were located by the close inspection of the distinct colour spots in which the defects appeared as dark holes. The LC interference colour was also correlated with the concentration of DNA with brightness of the spots increasing with increase in density of immobilized DNA. The least concentration of DNA that furnished a coloured spot was 0.5 µM, below this concentration only dark or grey spots were observed on microarrays due to homeotropic alignment of LC with the substrate. This strategy has advantages in quality assessment of DNA-based microarrays. Chen and Yang[66] demonstrated the effect of presence of divalent cations magnesium (Mg^{2+}) or calcium (Ca^{2+}) in the buffer solution using DNA-based LC sensor. DNA was added to a buffer solution containing magnesium chloride ($MgCl_2$) and then dispensed on DMOAP-coated solid surface. On applying 5CB LCs to the DNA immobilized self-assembled monolayer (SAM) surface, the disruption in the orientation of LC has been observed resulting in a distinct optical texture visible to the naked eye. It has been observed that by adding 100 mM $MgCl_2$ in the buffer solution, the lower limit of detection (LOD) of 4 µg ml^{-1} (or 40 pg for 10 nl of DNA sample solution) has been achieved. This fall in LOD value happened due to the screening of electrostatic repulsion of DNA molecules by Mg^{2+} ions in the sample solution which consequently increased the density of surface-immobilized DNA. This study has scope in development of quantitative biosensor for the ion detection in liquid and water samples.

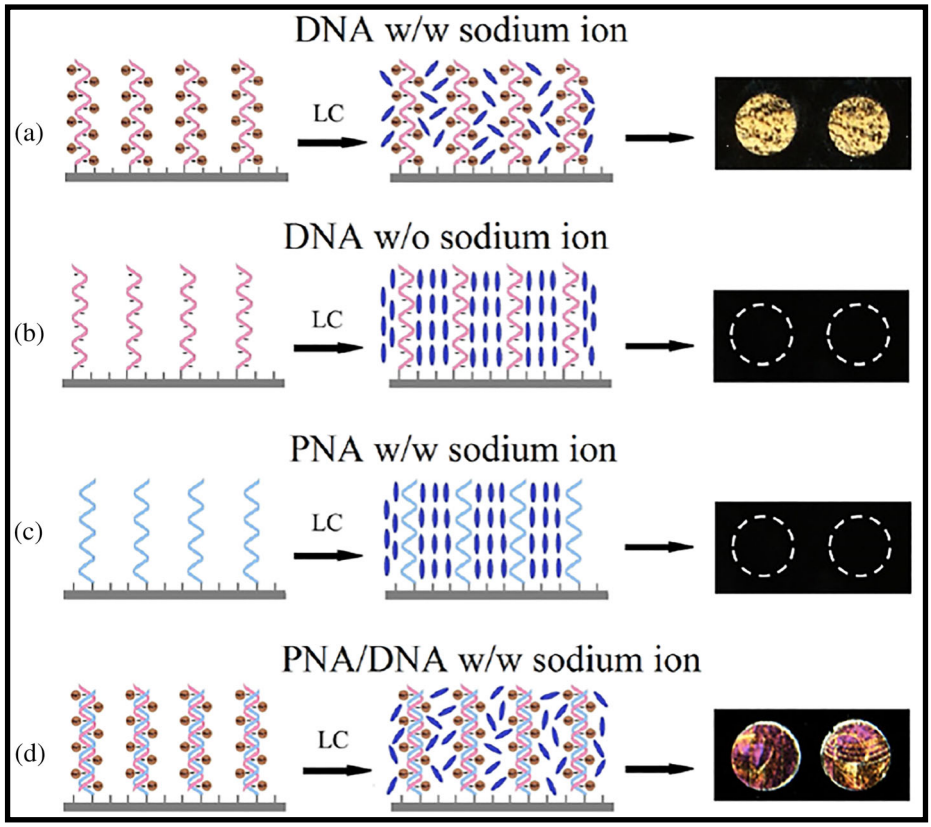

FIGURE 5 Principles for detection of DNA by using LC. Red probes represent DNA whereas blue probes represent PNA. (a) DNA contact with sodium ion, (b) DNA contact without sodium ion, (c) PNA contact with sodium ion and (d) PNA/DNA complex contact with sodium ion (adapted from Liu and Yang.[67] with permission from Elsevier)

The role of metal ions in the detection of DNA using LC was demonstrated by Liu and Yang.[67] It was observed that the LC orientation was switched from homeotropic to planar or titled in the presence of sodium (Na^+) ions immobilized on ultraviolet (UV) treated DMOAP surface. This phenomenon was then utilized in detection of DNA by immobilizing DNA on Na^+/UV-DMOAP surface. The negatively charged DNA molecules formed an electrostatic complex with Na^+ ions and disrupted the orientation of LC resulting in bright DNA spots (Figure 5). As the method is unsuitable for the detection of hybridization of specific DNA target on the surface due to the non-differentiating tendency of Na^+ ions to bind with both the probe and the target DNA, instead of DNA, an electroneutral peptide nucleic acid (PNA) was used as a probe to hybridize with specific DNA target. The modified LC cell detected a 600 base paired DNA target with a LOD of 10 fM.

A lot of attention has been focused on the enhancement of electro-optical, physico-chemical and dielectric properties of LCs for various applications by incorporating the suitable nanoscale dopants into the host-LC material.[107] The amplification of optical signal has been proposed by Yang et al.[68] by using gold-nanoparticles (Au-NPs) as signal enhancer for the detection of DNA. The DNA LC biosensing surface was generated by applying a mixed monolayer of (3-aminopropyl)trimethoxysilane (APS)/DMOAP on a glass slide to immobilize the DNA probe on it. The captured DNA probe along with the reporter DNA functionalized Au-NPs probe hybridized with target DNA as a function of concentration in sandwich format resulting in the optical change of LC biosensor from a dark appearance to a birefringence texture. The increase in sensitivity was attributed to the high areal density of DNA caused by the binding of a large number of DNA strands on the high specific area of Au-NPs. A significantly lower detection limit of 0.1 pM was achieved using this Au-NPs based signal enhancement method. Verma et al.[69] have utilized micrometer sized 5CB liquid crystalline droplets to detect ssDNA/dsDNA at aqueous–LC interfaces. The LC droplets with high surface area and high spatial resolution can act as highly sensitive medium for the optical detection of DNA. LC droplets were coated with positively charged poly(L-lysine) (PLL) using layer-by-layer technique. PLL strongly interacts with LC droplets and changes its alignment from bipolar to radial configuration. When negatively charged DNA is electrostatically adsorbed on the PLL coated LC droplets, the configuration again changes to bipolar from radial. The detection limit of the PLL-LC droplets towards ssDNA was found to be 50 nM. They further studied the controlled release kinetics of drug encapsulated ds-DNA adsorbed on PLL coated LC droplets using propidium iodide as a model drug. The results indicate that the drug releases in a controlled manner over time without changing its LC orientation configuration (Figure 6) as monitored through optical signal and fluorescence intensity measurement, which opens up a new venture for the development of DNA-based drug nanocarriers and controlled drug release of DNA-based drug delivery systems.

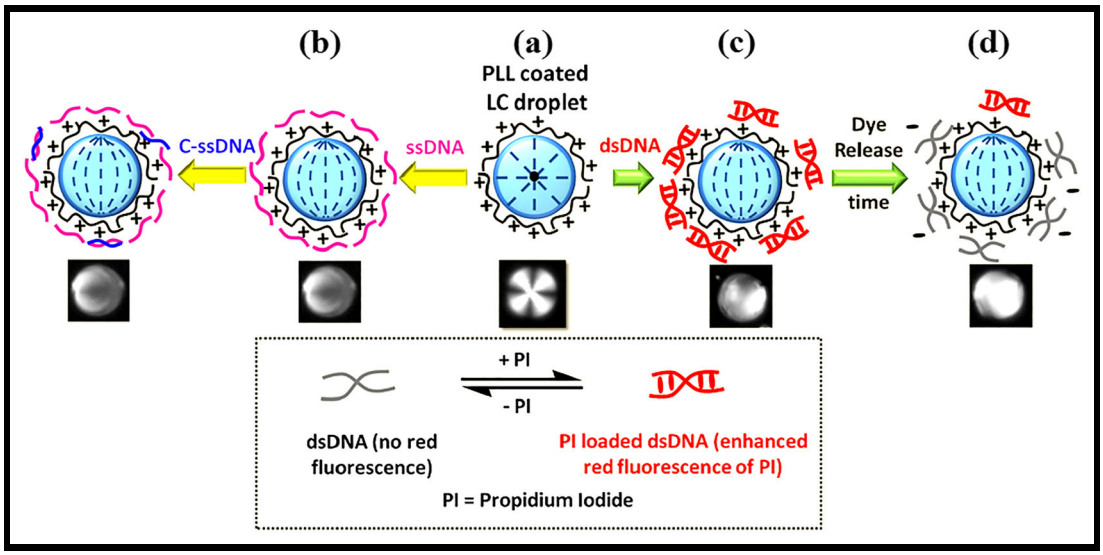

FIGURE 6 Schematic illustration showing radial configuration of (a) PLL coated LC droplet and bipolar configurations on adsorption with (b) ss-DNA, (c) dsDNA and (d) preservation of the LC droplets orientation configuration during propidium iodide release from its complex with DNA over time (adapted from Verma et al.[69] with permission from American Chemical Society)

FIGURE 7 (I) Schematic illustration of microfluidic channel for immunoassay; (II) LC based immunoassay developed in microfluidic channel, allowing test results to be observed with LC images taken under a polarized microscope (cross polars). (a) IgG-coated surface, (b) biotin-bovine serum albumin (BSA) coated surface and (c) schematic illustration of the level-free detection mechanism based on LC (adapted from Xue et al.[70] with permission from Wiley)

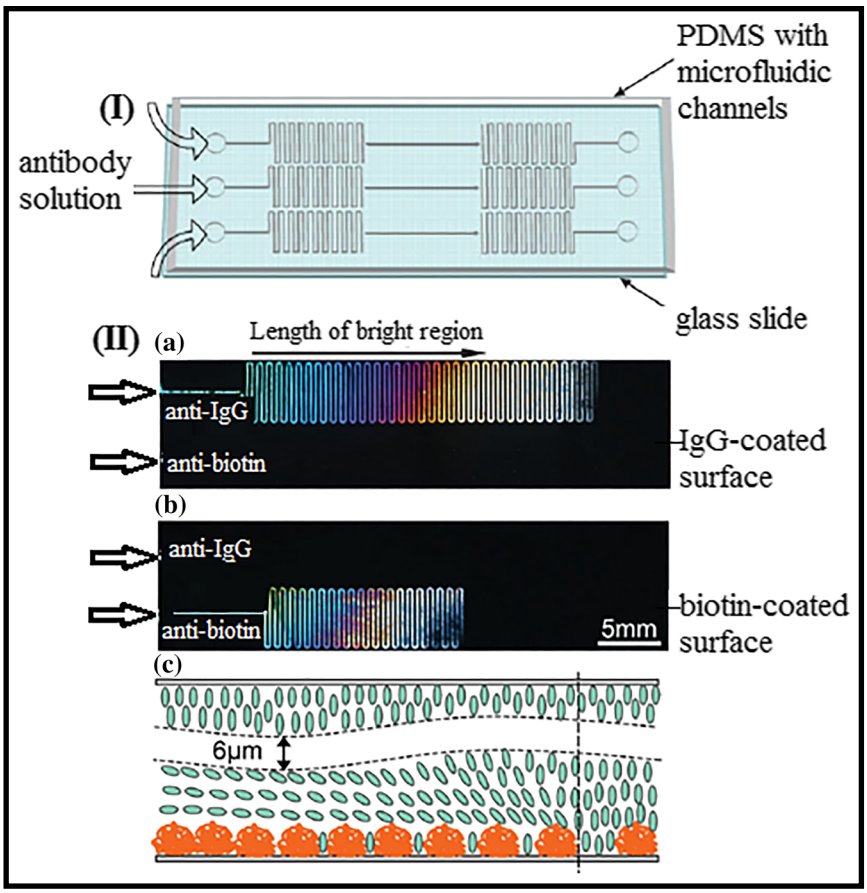

2.3 | LC immunosensor

Immunosensors are a class of solid-state devices and affinity biosensors in which the immunochemical response on specific recognition of antibodies and antigens is measured by coupling to a suitable transducer. In recent past, a lot of research work has been done by various groups to design liquid crystalline immunosensors for specific detection of biomarkers. The LCs must possess some properties to permit

specific binding between antigen and antibody such as (i) it must not denature the structure of antigens or antibodies, (ii) it should not combine with the binding domains of antigens or antibodies and (iii) the viscosity of the LC should be low so as to allow facile diffusion of antigens or antibodies into proximity of each other for binding interactions. Luk et al.[108] investigated five different classes of lyotropic LCs with different chemical functionality and molecular structures to establish that molecular structure plays a significant role in establishing the specific binding of antibodies with antigens. Out of ten lyotropic LCs tested for their probable use as birefringent materials to permit human immunoglobulin G (IgG) binding to surface bound anti-human IgG, only three lyotropic LCs, (i) cetyl pyridinium chloride (CPCl), (ii) tetradecyl dimethyl amineoxide (C14AO) and disodium chromo glycate (DSCG) have been found to facilitate the specific binding between antibody and antigen without denaturing them. Out of these three LCs, DSCG has been found to be the most permissible for specific binding of human IgG with anti-human IgG due to its low viscosity, high birefringence and biocompatibility. The binding event was visualized using a fluorescence microscopy technique, which showed bright circular domains on combination of fluorescein isothiocyanate (FITC)-conjugated anti-human IgG with human IgG. The main disadvantage of the method is the use of fluorescent probes in labelling the antibodies which requires an additional preparation step and limits the possibility of formation of point-of-care applications. In this context, Xue et al.[70] developed a label-free microfluidic immunoassay by exploring the interactions between LCs and antibodies. IgG was coated on the DMOAP-modified glass slides and a buffer solution containing anti-IgG was pipetted into microfluidic channels placed on them (Figure 7(I)). After 30 min of incubation the IgG-sample glass slides were rinsed with buffer and dried under a nitrogen stream and LC optical cells were prepared by aligning the IgG-sample and DMOAP-modified glass slides separated by a fixed distance of 6 μm using a pair of Mylar films at two ends of the glass slides. On injecting LCs in the space between the two plates through capillary effect, bright optical signals were observed on specific binding sites of anti-IgG–IgG interaction (Figure 7(II)) and based on the optical textures, the anti-IgG concentration as low as 0.02 mg ml^{-1} could be detected. This microfluidic LC-based immunoassay was further utilized to detect various biomaterials such as anti-IgG, anti-biotin, and their mixtures simultaneously with high specificity and high sensitivity.

Zapp et al.[71] used electroactive ionic LC thin films to develop electrochemical immunosensor for the quantitative detection of cardiac biomarker myoglobin (Mb). On a glassy carbon electrode, ionic LC (E)-1-decyl-4-[(4-decyloxy phenyl)diazenyl]pyridinium bromide (Br-Py) was coated using a drop-cast method. On polyethylene imine coated gold nanoparticles modified Br-Py/GCE electrode (AuNP-PEI/Br-Py/GCE), Mb antibody was covalently immobilized using glyoxal as a crosslinker. Mb antigen was detected electrochemically using the ab-Mb/AuNP-PEI/Br-Py/GCE electrode in the wide range 9.96–72.8 ng ml^{-1} using electrochemical impedance spectroscopy with a correlation coefficient of 0.995 and LOD value of 6.29 ng ml^{-1}. The authors have also tested the reproducibility of the immunosensor by performing inter-assay variation tests using five immunosensors and found a relative deviation of 4.3% among them. The specificity of the sensor was tested by performing interference studies with different analytes viz. ascorbic acid, glucose, creatinine, dopamine and uric acid. Less than 10% of interference was observed for all the potential interferents studied with respect to control test. The advantages of the immunosensor include its good precision, simple design, low LOD value and high accuracy while the drawback is that tests with real samples are required for routine clinical tests. The LC based biosensing system was modified to a more sensitive system by Lee et al.[72] by using LC microdroplets as recognition matrix instead of LC molecules on solid surface. Microdroplets-based LC biosensor has provided reasonably high sensitivity because of their high mobility, smaller size and high surface area. The 5CB nematic LC microdroplets were stabilized in radial configuration by using sodium dodecyl sulphate (SDS) as surfactant. The amphiphilic block copolymer (poly(styrene-b-acrylic acid)) (PS-b-PA) was used as a modifier to control the orientation of the 5CB microdroplets. A weight ratio of 5:1 for PS-b-PA to SDS was found to be an optimum ratio for the stabilization of microdroplets of the size ranging between 10 to 30 μm. Goat anti-IgG molecules were anchored on the microdroplets (Figure 8) and were used for rabbit IgG detection over a concentration range of 20 to 1000 ng ml^{-1} in phosphate-buffered saline (PBS) and in other media such as 10% blood plasma and 10% fetal bovine serum (FBS) solution. The LOD of this immunosensor was found to be as low as 16 ng ml^{-1} with a response time of 30 min, which is a three times faster response than what was obtained in blood plasma and FBS. The technique so developed after proper optimization has scope for the non-invasive sensing of biomarkers in biological fluids.

3 | APPLICATIONS AND ANALYTICAL PERFORMANCE OF LC BIOSENSORS

LC biosensors work on the principle of change in orientation of liquid crystalline molecules induced by specific binding of biorecognition molecules with target analytes. LC biosensors have attained a lot of attention in recent years due to their potential advantages in terms of reaction mechanism, sensitivity, simplicity, efficient, and portability, etc. The LC biosensors are of growing interest in various applications such as detection of proteins, virus, bacteria and clinically relevant reagents, heavy metals ions and environmental organic pollutants as categorized schematically in Figure 9.

3.1 | Protein detection

Proteins are macromolecular nitrogenous organic compounds which consist of long chains of amino acids linked through peptide bonds. They are required by living organisms for cellular functions such as enzymatic activity, mechanical and structural activities, cell signalling and immuno response, etc. LC compatibility with biological material and its ability to amplify and transduce protein binding event makes it pertinent for the development of biosensors. Proteins can adsorb on

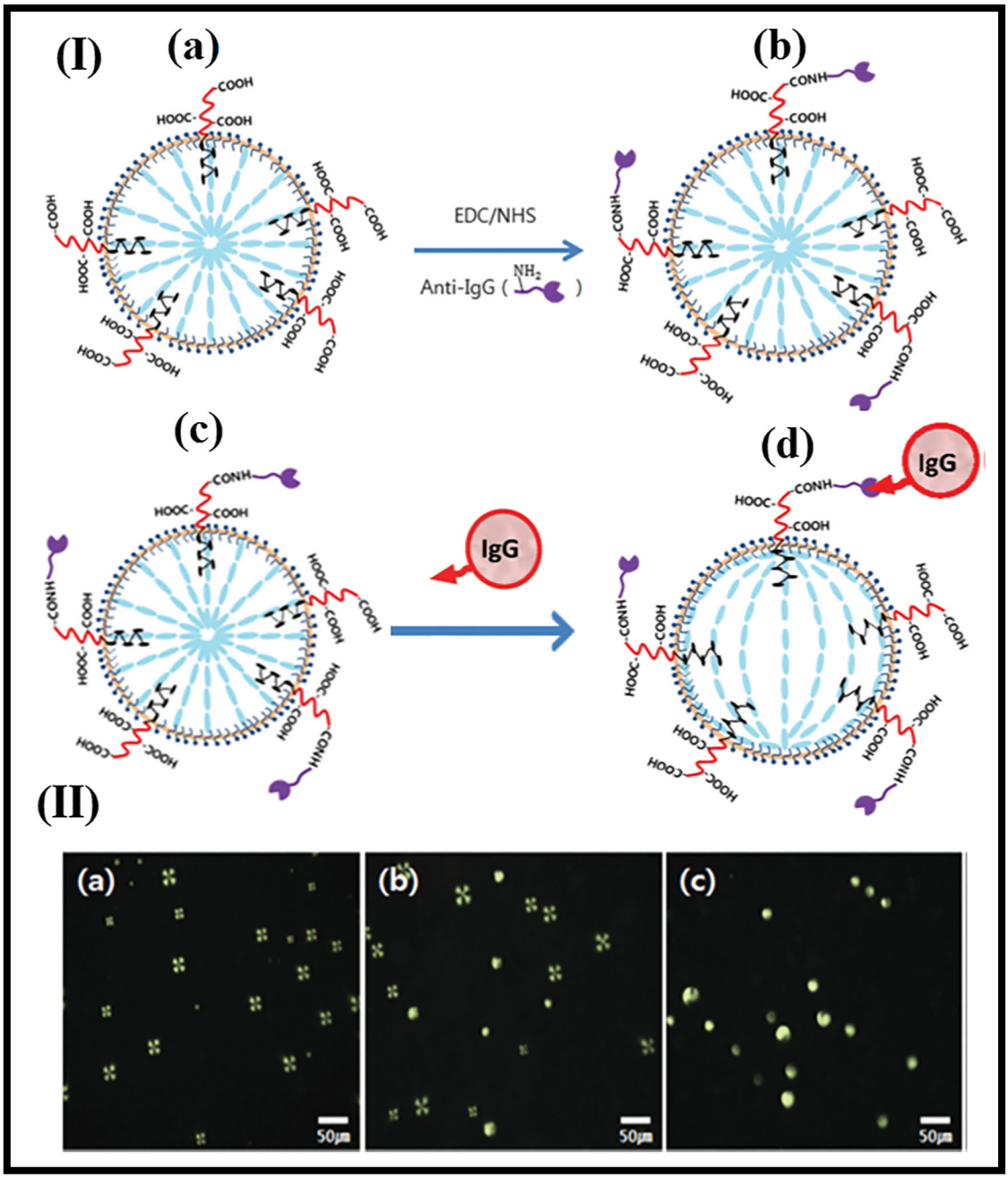

FIGURE 8 (I) Orientational state of 5CB in LC microdroplets before (a) and after (b) anchoring anti-IgG; orientation state of 5CB in anti-IgG-anchored LC microdroplets before (c) and after (d) interactions with IgG. (II) Polarized microscopic images of anti-IgG-anchored LC microdroplets incubated in PBS having different concentrations of IgG at constant density of LC droplets (9×10^3 microdroplets ml^{-1}) anchored with 5 μg ml^{-1} of anti-IgG. Contact time 30 min. [IgG] = (a) 10 ng ml^{-1}, (b) 20 ng ml^{-1} and (c) 50 ng ml^{-1} (adapted from Lee et al.[72] with permission from Royal Society of Chemistry)

hydrophobic interfaces of LCs and can act as mediator to a range of biological interactions occurring at LC interface. The important biological interaction of proteins such as protein–ligand and protein–protein interactions can be monitored by observing the orientational changes that occur in thermotropic LC on binding events of protein.

The use of LC for the monitoring of protein binding on a chemically functionalized surface was demonstrated for the first time by Gupta et al.[28] They exhibited a label free method in which a thin film of diagonally deposited polycrystalline gold was chemically functionalized with a mixed SAM of biotinylated thiol $[(CH_2)_2O]_2NHCO(CH_2)_{13}SH$(BiSH) and octyl mercaptan (C_8SH). The 5CB nematic LC was used to transduce and amplify the binding event of biotin to avidin through readily observable optical transmittance response when inserted in the cell made of two SAM surfaces separated by a thin plastic film (Mylar sheet). The specific binding of avidin to biotin present in mixed SAM leads to the masking of anisotropic

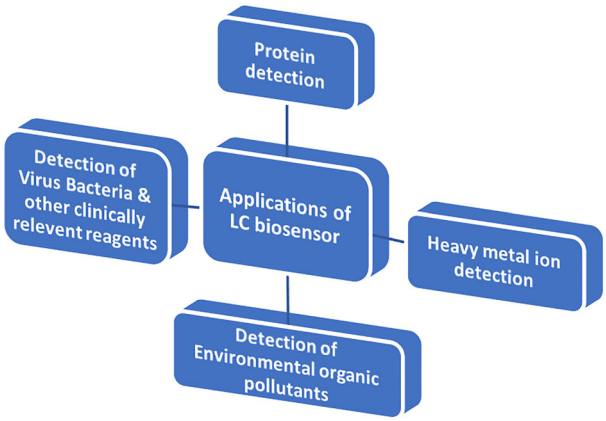

FIGURE 9 Schematic categorization of LC biosensor applications in various field

roughness of gold film and thus tuning the orientation of bulk LC. They further observed that by tuning the surface topography of the gold films, it can be used to capture an antibody by a surface immobilized protein. Further, avidin bound antigen was immobilized on the SAM functionalized gold surface and was used to quantify anti-Av-IgG in the solution. The assembly described in the article was able to detect a concentration as low as 2.3 nM of anti-Av-IgG (Table 1). Another label free LC based sensor was reported by Skaife and Abbott to quantify the immunoglobulin binding (IgG) on a surface-bound biotin antigen.[53] A mixed SAM of organosulphur compounds was formed on the surface of semi-transparent gold films deposited on titanium enriched glass substrate. The 5CB nematic LC film confined between two SAMs was used as a surface-sensitive agent for the quantification of the protein binding. The alteration generated in the grayscale brightness of LC due to the binding of IgG was used to quantify the protein binding on the surface. The average luminescence, calculated from the grayscale image of LC cells, increased as a sigmoidal function of the amount of bound IgG and the analysis was carried out over a concentration range 1–100 nM of IgG in solution using a CCD camera. It was also established that optical response of LC to the attachment of IgG on the surface was largely controlled by the mass transport phenomena. As the binding of biomolecules on a sensing platform is very critical for highly sensitive optical detection, the effect of orientation of immobilized proteins on their binding ability was studied by observing the optical appearance of 5CB nematic LC based cells as shown by Luk et al.[109] SAMs of alkanethiols were formed on thin films of gold uniformly deposited on titanium enriched glass substrate. The influence of preferential orientation of immobilized RNase A for high protein binding characteristics over random orientation (Figure 10) has been investigated in the orientation of 5CB LCs placed on these surfaces. The binding of the targeted protein Ribo nuclease inhibitor (RI) to the RNase in identical interfacial microenvironments was characterized by measuring the bound protein layer thickness using ellipsometer and through orientational changes of the LC caused by the disruption of surface alignment on protein-receptor binding.

Results showed that the binding of RNase to RI increased by four times with a preferential orientation in comparison to random orientation of the receptor molecules on the surface. The increased protein binding on the surface leads to a larger optical change in the LC alignment (Figure 10(II)) thus makes it an attractive technique for the development of a rapid biosensor. The effects of areal density and the size of biomolecules on the time required for LC in contact with the modified surface to exhibit uniform alignment was investigated by Clare and Abbott.[110] They have reported a strategy to modify liquid crystalline interfaces with self-assembled monolayer modified peptides onto gold substrates to study and amplify the range of peptide-liquid crystal interface phenomenon. Peptide sequence for Src-tied protein kinase and its synthetic equivalent after kinase modification were immobilized on oligoethylene glycol containing SAMs formed on a gold substrate. For the determination of optimal areal density of peptides, LC cells were created by sandwiching 5CB material between two substrates with varying densities. The relative areal densities of the peptides at the interface were characterized by using polarization modulation-infrared reflectance absorbance spectroscopic technique. It was found that the surface with low peptide areal density (1% or low) shows line defects due to the disruption of the LC alignment caused by the peptides. These line defects were removed after annealing the samples at 36°C for 17 h and then cooling, leading to the appearance of preferred orientation of 5CB LC. The effect was absent in the case of higher areal densities of 5 to 100% even after a long duration of time (100 h) suggesting that reorganization of 5CB LC to exhibit long-range orientation ordering is time dependent and it increases with increase in areal density of peptide. It has also been reported that the time required for uniform anchoring depend on areal density of peptides, presence or absence of the peptides onto the surface. This study has technological futuristic implications in the design and fabrication of label free LC sensors for imaging the protein binding at interfaces. Govindaraju et al.[73] quantified proteins captured on the surface decorated with oligopeptides by measuring anchoring energy of LCs with thin gold surfaces containing organothiol. The anchoring energy is calculated by applying known magnitude of mechanical torque to the liquid crystalline cell and then measuring the resulting response as the change in orientation of the LC. The cell surface was decorated with a cancer associated peptide sequence from epidermal growth factor receptor (EGFR) and then incubated in solutions containing different concentrations of the anti-phosphotyrosine IgG antibodies. Measurements showed a systematic reduction in anchoring energy of 5CB from 4.4 to 1.4 μJ m^{-2} on increase in amount of captured antibody from 10 pM to 100 nM (Table 1). This technique is not only a simple method for the determination of protein binding interactions but it also showed the application of LCs in detecting such a low concentration of protein. The identification of optimal range of interaction (anchoring) energy required for a measurable change in LC orientation on binding of protein was reported by Lowe et al.[74] It is to be noted that when surface-induced ordering of LC is used to report the presence of proteins adsorbed on surfaces, low anchoring energy surfaces are desirable. Twisted nematic 5CB were used to form the optical cell and the corresponding twist angle was used for the

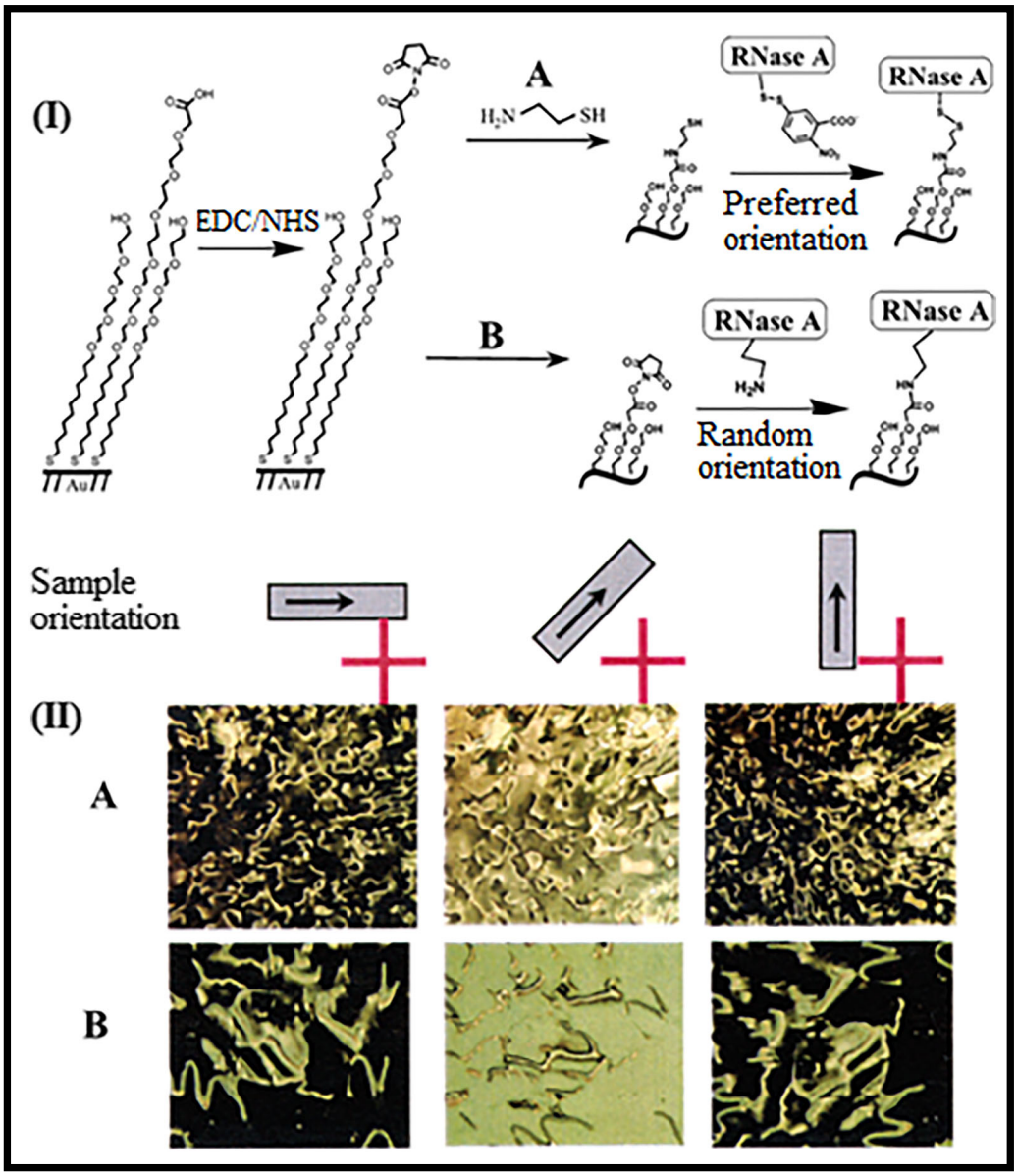

FIGURE 10 (I) A SAM presenting a mixture of carboxylic acid groups and tetra(ethylene glycol) groups is activated by ethyl(dimethylaminopropyl) carbodiimide (EDC) / N-hydroxysuccinimide (NHS) to form a monolayer presenting an NHS ester. RNase A is immobilized via the activated SAMs with either a unique orientation (A) or random orientations (B). (A) The NHS-activated SAMs are coupled with 2-aminoethanethiol to present thiol groups on the surface. The thiol groups selectively couple with the 2-nitro-5-thiobenzoic acid (NTB)-protected cysteine residue of A19C RNase A, forming a covalent disulphide bond to afford RNase A immobilized with a unique orientation. (B) The amino groups of lysine residues and N-terminus of the wild-type RNase A directly couple to the NHS-activated acid on SAMs to afford immobilized RNase A without a unique orientation. (II) Optical images (crossed polarizers) of nematic 5CB sandwiched between nanostructured surfaces that support (A) RI bound to preferentially oriented RNase A and (B) RI bound to randomly oriented RNase A (adapted from Luk et al.[109] with permission from American Chemical Society)

calculation of anchoring energy, which was further correlated with the loading of protein molecule on the surface. EGFR was covalently attached on chemically functionalized polydimethylsiloxane (PDMS) stamps and then by using the affinity contact printing, EGFR was transferred to self-assembled monolayers of amino tetra(ethylene glycol) terminated alkane thiol functionalized gold films, which leads to the decrease in the anchoring energy and thus changing the orientation of the LC. The research described that for LC based biomolecular detection, the optimal anchoring energy of the surfaces should be in the range of 2.0 to 0.5 μJ m^{-2}. The anchoring energy values outside this range resulted in uncertainty in measurement of twist angle of LC leading to large errors. The methodology so developed in this article permitted the use of LCs to report surface mass densities of EGFR as low as 30–40 pg mm^{-2}. Sharma et al. have designed a LC biosensor for the quantitative detection of bovine serum albumin (BSA) protein.[75] A change in the homeotropic alignment of nematic LC into

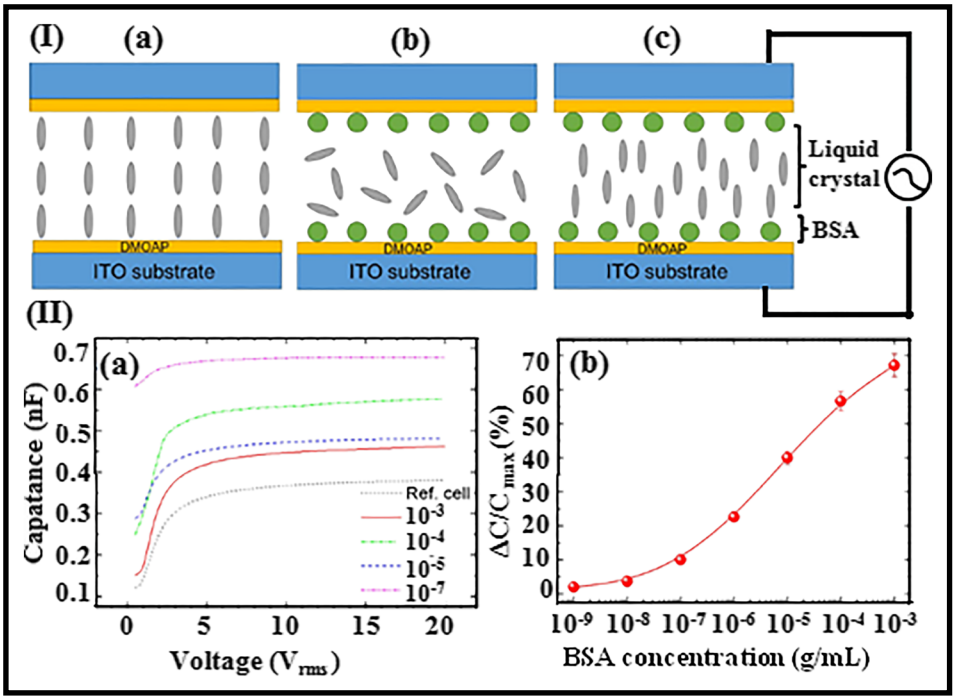

FIGURE 11 (I) Schematics of LC biosensor (a) LC molecules in homeotropic alignment in the absence of BSA, (b) disrupted orientation of LC in the presence of BSA and (c) reorientation of LC molecules under applied external alternating current field and the original alignment can be restored at high voltage. (II) (a) The capacitance–voltage curve in the presence of various concentrations of BSA (in g ml^{-1}) immobilized on DMOAP-coated ITO-glass plate, (b) the electric capacitance parameter $\Delta C/C_{max}$ [$\Delta C = C_{max}$ (maximal capacitance at $20V_{rms}$) – C_0 (initial capacitance at $0.5V_{rms}$)] as a function of the BSA concentration (adapted from Lin et al.[76] with permission from American Institute of Physics)

homogeneous phase was observed in the presence of BSA. This change in the LC orientation is caused by the absorption of BSA on the carboxyl functionalized gold nanoparticle/silane surface changing the substrate surface energy as monitored by contact angle measurement and detected an ultra-low concentration of 0.5 μg ml^{-1} BSA.

In addition to optical detection techniques, Lin et al.[76] have demonstrated the detection and quantification of biomolecules by electro-optical technique. BSA was quantified on indium tin oxide (ITO) coated glass substrates modified with DMOAP used as a vertical alignment in a cell using eutectic nematic mixture LC by a unique electric capacitance measurement technique. The influence of biomolecules on the electric capacitance in a parallel-plate-capacitance structure was investigated. The mechanism involved an alteration in electric capacitance due to disruption of LC orientation by BSA as the anchoring strength of DMOAP to LC gets weakened, which under significant external voltage could be restored to original homeotropic alignment (Figure 11(I)). The BSA is quantified by measuring the voltage dependent electric capacitance ($\Delta C/C_{max}$) as a function of BSA concentration (Figure 11(II)b) as higher voltage is required to restore the vertical alignment from larger disrupted LC orientation caused with increasing concentration of immobilized BSA. A lowest detection limit of 15 pM BSA concentration could be achieved with this opto-electric LC biosensor.

In a further development, Wu et al.[77] have proposed the use of azobenzene based LC molecules which are chemically modified with two azo groups as chromophores for the detection and quantification of BSA protein. In this method, the dichroic dye sensitized LC (DLC) was aligned homeotropically on DMOAP surfactant coated ITO glass substrate. The non-covalent adsorption of BSA to DMOAP at the interface of DLC changed the orientation of dye sensitized LC molecules from homeotropic alignment state to disrupted state which was observed through the change in transmission spectra as a function of concentration of BSA. The transmittance at 470 nm has been found to decrease by increasing concentration of BSA immobilized onto the substrate. When no external field is applied ($V = 0V_{rms}$) due to disruption of LCs molecules by immobilized BSA, which become reoriented under high applied electric field resulting in increased transmittance and attain a plateau at $V = 10V_{rms}$ in a DLC cell. This novel biosensing technique utilizing the electro-optical properties of dichroic DLC was able to discern the BSA concentration linearly between 1 to 7.5 μg ml^{-1}.

A dual frequency liquid crystal (DFLC) based biosensor has been developed for the first time by Lin et al.[78] for label free protein quantification due to its tendency to show frequency reversible dielectric anisotropy behaviour. A DFLC comprises of a mixture of LC whose dielectric constant component parallel to the nematic director exhibits negative dielectric anisotropy at high frequency and positive at low frequencies. DMOAP surfactant used in this study for the assembly of LC cell serves the dual purpose as homeotropic aligner for DFLC and as an interface media for the non-specific adsorption of BSA. The dielectric anisotropic behaviour of DFLC in the presence of adsorbed BSA was analysed by assessing the response (real part of dielectric permittivity) as a function of BSA concentration at two different frequencies (200 Hz and 100 kHz). At 100 kHz, the dielectric constant $\acute{\epsilon}$ values have been found to increase with increasing concentration of BSA while at 200 Hz the values were found to decrease by increasing concentration of BSA. This methodology of protein assay provided the quantification of BSA over a wide range of concentration from 10^{-2} to 10^{-7} g ml^{-1}. Temperature dependent spectroscopic interactions and docking analysis of LCs and proteins has been studied by Kalita et al.[111] to investigate the dynamics of director transfigurations of the LC molecule on its interaction with human serum albumin

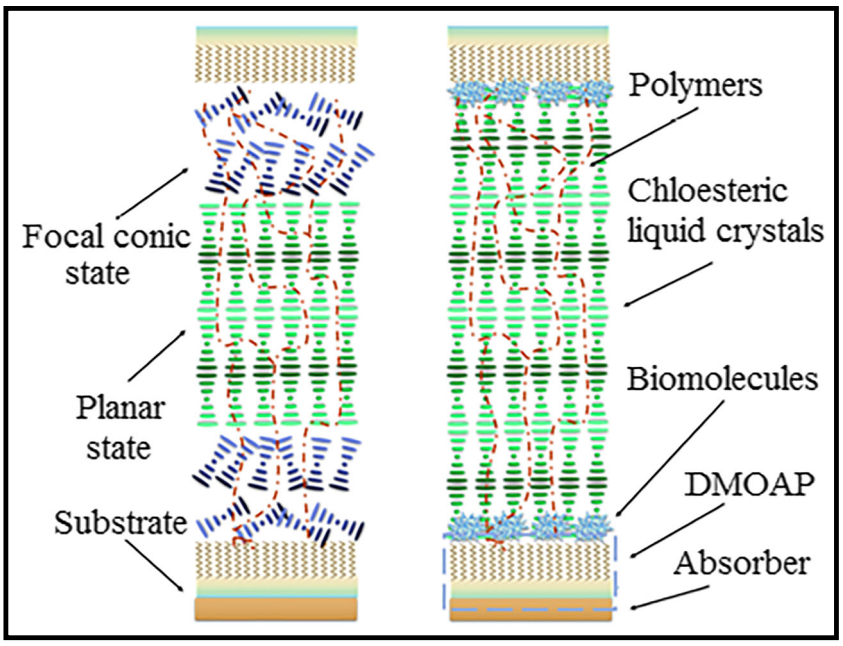

FIGURE 12 Schematic of the polymer stabilized cholesteric structure biosensor. The configuration changes from FC to P-state in the presence of biomolecules on the DMOAP substrate (adapted from Chuang et al.[79] with permission from Dove Medical Press)

(HSA) in a LC cell. The vibration properties of the interaction between LC and HSA was determined with the help of Raman spectra, whereas the binding sites of 5CB LC on HSA along with binding energy were revealed by molecular docking analysis. This technique provides a simple and effective tool for the detection of biomolecules and chemical events through LC–protein interaction as a function of temperature. Recently, polymer stabilized cholesteric liquid crystal (PSCLC) has been used for fabrication of label-free smart phone based LC biosensor on the ceramic silicon constructed DMOAP platform for the detection of BSA.[79] The polymer (2.9% R5011; Merck) stabilized cholesteric LCs (CLCs, E7; Merck) structure shows sensitive interfacial effects on the alignment layer of DMOAP coated-glass substrate. The CLCs aligned vertically near the DMOAP surface and planner in the bulk, exhibiting the focal conic and a planar state in the near surface and bulk region of the PSCLC cell device, respectively. The biosensing mechanism of PSCLC device is based on the change in the molecular arrangement of CLCs from FC to P-state with increasing concentration of immobilized BSA (Figure 12), leading to the colour-indicating characteristic of the PSCLC device. The texture is imaged in a smartphone set on a stage with its camera aligned with a set of lens fixed in the designated stage. The chirality of CLCs have been found to be highly sensitive to BSA concentration on the DMOAP alignment layer on ceramic silicon platform, with colour changes observed through a smartphone camera. The PSCLC-biosensor has also been employed to detect BSA in urine samples to demonstrate its applications for clinical applications. Correlation has been reported in the colour intensity of the sensor with respect to BSA concentration indicating the potential over a wide range of detection from 1 ng ml^{-1} to 2 mg ml^{-1} with a LOD close to 1 ng ml^{-1} BSA in urine samples, which is nearly comparable to a that of a commercial biosensor, proving it to be a sensitive, quantitative and economical platform for sensing based on the colour modulation on a smartphone.

3.2 | Detection of virus, bacteria and other clinically relevant reagents

LCs have been used as potential sensors for the detection of various microorganisms such as virus[112–114] and bacteria.[115] This detection is very useful in the current scenario for safeguarding public health. It has also been shown that the interaction between phospholipid and liquid crystalline mesogenic phases can result in change in the LC orientation which can be viewed through polarizing optical microscope under crossed polarizers. Virus as well as bacteria are encapsulated by lipid membranes so their interaction with LC can trigger transition in LC orientation. The different types of bacteria and viruses were detected and differentiated based on their cell-wall envelope structure using 5CB monodisperse LC emulsion droplet by Sivakumar et al.[49] Two different types of bacteria (Gram positive and Gram negative) and viruses (enveloped and non-enveloped) were distinguished on the basis of change in LC orientation. The enveloped virus and Gram-negative bacteria both contained an outer lipid membrane and on interaction with the LC droplets, there is transfer of lipids from the organisms to the interface of LC. This triggered the change in orientation from bipolar to radial within the LC droplets. There is no such change observed in LC orientation in case of Gram-positive and non-enveloped virus due to absence of lipid membrane. The method proposed was able to detect small number of *Escherichia coli* bacteria ($1–5 \times 10^5$ cells ml^{-1}) and low concentration (10^4 pfu ml^{-1}) of Influenza A virus. This versatile sensing method can be used to develop a screening assay for a large number of bacteria and viruses based on their cell wall structural features.

Based on the earlier principle, Wei and Jang[116] developed a LC sensing platform for imaging the interaction between chitosan grafted graphene oxide (CS-GO) and the phospholipid membrane. CS-GO nanomaterials were prepared by covalent linkage between carboxyl

(–COOH) groups of graphene oxide nanosheets and amine ($–NH_2$) groups of chitosan. The interaction of CS-GO film with negatively charged phospholipid [dioleoyl-sn-glycero-3-phospho-rac-(1-glycerol) sodium salt (DOPG)] was observed using 5CB nematic LC based cell. Initially, when phospholipid monolayer was formed on LC cell, it resulted in a dark appearance due to the homeotropic orientation of 5CB molecules at the aqueous/LC interface. On applying CS-GO nanomaterial, the interaction between the phospholipid monolayer and the nanomaterial leads to the de-structuring of DOPG membrane which changed the orientation of LC molecules from homeotropic to planar state just after 10 min of interaction. For observing antibacterial activities of the CS-GO nanomaterial on *E. coli* cells sessile LC microdroplets were used. The interaction of CS-GO with live *E. coli* cells lead to the transfer of lipids from *E. coli* cells to the LC droplets generating dark textures due to the radial configuration (homeotropic orientation) of LC cell. On the contrary, the inactivated *E. coli* cells have illustrated a distorted bright fan-shaped texture (planar orientation) on interaction with CS-GO. Kim et al.[41] have fabricated a label-free 5CB nematic LC-based *mycobacterium tuberculosis* (TB) immunosensor that does not require any complicated preparation of clinical specimens and obscured instrumentation. A nanostructured surface comprising of thin film layers of titanium (Ti) and gold (Au) obliquely deposited on glass slides was used as a substrate to immobilize the TB-antigens. The nanostructured surface was functionalized with carboxyl groups by using mixture (7:3) of 11-mercapto undecanoic acid and 1-decanethiol which was later activated using NHS/EDC to immobilize TB-antigens on it. The non-specific binding sites on the nanostructured surface were blocked using ethanolamine and then clinical specimens were incubated on the surface. The binding of antibody to antigens masked the anisotropic surface topography and causes the disruption of orientation of LCs which changes the texture of LCs that was observed using a polarized light microscope. The diagnostic sensitivity of the immunosensor was found to be 76% and specificity towards TB diagnosis was 91%. In a similar approach, Su et al.[80] have developed a non-labelled LC biosensor for the detection of human β-defensin-2 (HBD-2), which is a type of induced defence element and is expressed in human lung, gastrointestinal tract, saliva and lacrimal gland. It is a key mediator of immunity and shows killing effect to viruses. Antigen HBD-2 was covalently immobilized on the glass substrate via the bonding of aldehyde group of DMOAP/(3-aminopropyl)trimethoxysilyl chloride/glutaraldehyde to the amino group of HBD-2. On specific binding of antibody to the immobilized antigen, the homeotropic alignment of LC changes to tilted transition which produced a visible optical change under cross polarized light. This change in grayscale intensity showed a linear variation with respect to concentration of HBD-2 antibody in the range from 1 to 10 ng ml^{-1}. The immunosensor showed high selectivity when tested against targets of HBD-2, HBD-3, BSA and cecropin B with LOD value of 0.53 ng ml^{-1}. This approach has implications in designing an LC based sensor for the detection of a variety of antimicrobial peptides. On the same principle, a pH sensitive microfluidic LC based sensor for the detection of urea has been fabricated by coating the 5CB LC droplets with poly(acrylicacid-b-4-cyanobiphenyl-4-oxyundecylacrylate) (PAA-b-LCP). At the LC–water interface and immobilizing urease on the PAA chains through covalent bonding. The change in pH resulting from the catalytic conversion of urea by urease leads to change in orientation of $5CB_{urease}$ droplets from bipolar- to-radial orientation, when viewed through crossed polarizers. The LOD value for this urea biosensor was found to be 3 mM with a response time of 180 s. An enzymatic cholesterol biosensor was fabricated by Tyagi et al.[81] using cholesterol oxidase (ChO_x) enzyme immobilized on SAM of DMOAP and (3-aminopropyl)-trimethoxysilane (APTMS). Glutaraldehyde was used as a crosslinker to bind ChO_x to DMOAP/APTMS on a glass slide and these glass slides were used in making 5CB cells. The addition of cholesterol to the DMOAP/APTMS/Glu/ChO_x LC cell changed the alignment of the LC from homeotropic to homogeneous due to oxidation of cholesterol to cholest-4-en-3-one that brings about changes on the surface topology. The scanning electron microscopy (SEM) images showed that the oxidation of cholesterol led to the formation of nanocups like structures which resulted in enhanced non-uniform surface of SAM causing disruptions of LC molecules. It was found that the higher the concentration of cholesterol, more was the disruption resulting in greater tilting of LC molecules. The study showed the cholesterol detection in the range of 10 to 250 mg dl^{-1} using this technique.

Alzheimer's dementia (AD), a common disease in elderly people is related to a low level of neurotransmitter acetylcholine (ACh). ACh is hydrolysed by acetylcholinesterase (AChE) enzyme, which plays a key role in the regulation of the neural response system. A specific and sensitive detection of AChE by LC is reported by Wang et al.[82] using a cationic surfactant myristoylcholine chloride (Myr) decorated 5CB LC interface. The 5CB LC was impounded in a copper grid which was put on an octyl trichloro silane (OTS) treated glass slide. The enzymatic hydrolysis of Myr by AChE led to the formation of myristic acid and choline which induced a transition of LCs from homeotropic (dark) to planar (bright) orientation. The stability of the formed cationic surfactant monolayer was found to be dependent on the pH at the LC–aqueous solution interface with pH of 5.2 or 9.0 producing bright domains while the pH of 6.2 or 8.2 generating dark domains. Hence, the enzymatic study was performed in PBS buffer (pH 7.4) considering both the stability of Myr monolayer as well as the optimal pH of the enzymatic activity. The specificity study of the sensor using BSA and cellulase enzyme did not produce any optical change showing that there is no effect of these enzymes on Myr monolayer supported on the LC interface. The group also studied the effect of AChE enzyme inhibitor, Neostigmine on the optical properties of the LC corresponding to enzyme inhibition and found that the retarded activity of the enzyme impeded the change of optical appearance in LC. The detection limit of inhibitor was found to be 1 fM and for AChE it was around 0.000827 U ml^{-1} in the aqueous solution of serum albumin. Xu et al.[83] have reported a diagnostic kit based on thermotropic LC (E7) for the ultrasensitive detection of severe acute syndrome-coronavirus-2 (SARS-CoV-2) responsible for pandemic coronavirus disease 2019 (Covid-19). A cell was prepared using two glass plates with a bare one and another with a Dimethyloctadecyl [3-(trimethoxysilyl)propyl]ammonium chloride (DMOAP) coating

separated with a 2 mm PDMS spacer enclosing a copper grid filled with E7, which was adsorbed with a cationic surfactant, dodecyltrimethylammonium bromide (DTAB) that allows perpendicular anchoring of LC at LC–aqueous interface. The ssDNA probe (15-mer-5′-GCATCTCCTGATGAG-3′) was added over the DTAB-laden E7, that decreases the effective DTAB coverage causing LC towards a planer tilt which upon further interaction with target 15-mer SARS-CoV-2 ssRNA ($ssRNA_{CoV}$) (5′-CUCAUCA GGA GAUGC-3′) oriented again to a homeotropic alignment due to $ssDNA_{probe}$–$ssRNA_{CoV}$ hybridization, leading to the ultrasensitive detection of target ssRNACoV from pM to fM concentration (Figure 13). The device could detect as low as 30 fM concentration of $ssRNA_{CoV}$ with a smart phone-based application.

Recently a LC biosensor utilizing a specific DNA apatamer as probe has been reported for the detection of amoxicillin (AMX) antibiotic.[84] The specific-binding of AMX with an apatamer brings about conformational changes in the DNA causing disruption in homeotropic orientation of 5CB resulting in a visible optical change under a POM with a lowest detection limit of 3.5 nM. More recently, another LC biosensor for the detection of cardiac biomarker, troponin I (cTnI), has been reported based on immunoreaction with specific antibody using 5CB LC. The homeotropic orientation of LC gets disrupted due to the formation of antigen–antibody complex formation between cTnI and anti-cTnI, showing bright visual texture under POM with a lowest detection limit of 1 pg ml^{-1}.[85]

3.3 | Heavy metal ion detection

The main challenges in the utilization of LC materials for the detection of toxic heavy metal ions in liquid samples are: (i) only a high concentration (> μM) of toxic ions can produce observable LC transition,[117,118] (ii) problem of selectivity due to similar charge to size ratio of many metal ions and (iii) small size of ions leading to high mobility in bulk phases. A label-free LC biosensor was designed by Yang et al.[86] to enhance the capability of metal ions disturbing the orientation of LCs, for the selective and sensitive detection of mercury (Hg^{2+}) ions. The sensing strategy utilizes the binding property of Hg^{2+} ions with two DNA thymine (T) bases of the specific oligonucleotide of heparin structure to form a duplex like structure, which consequently hybridized to a complementary capture DNA probe immobilized on triethoxy silyl butyraldehyde/DMOP modified substrate that resulted in a distortion in LC orientation providing an enhanced visual image under POM for sensitive detection as low as 0.1 nM Hg^{2+} concentration. Singh et al.[87] have developed a dithiocarbamate ligand-based LC sensor for the real time detection of Hg^{2+} ions in water. In this work, amphiphilic potassium *N*-methyl-*N*-dodecyl dithiocarbamate (MeDTC) was synthesized and utilized to selectively bind toxic Hg^{2+} ions in trace amounts by forming a chelated complex between dithiocarbamate groups of MeDTC and Hg^{2+} ions. The sensor was fabricated by placing copper TEM grids on an OTS treated glass slide and then filling it with 5CB LC doped with MeDTC. It was

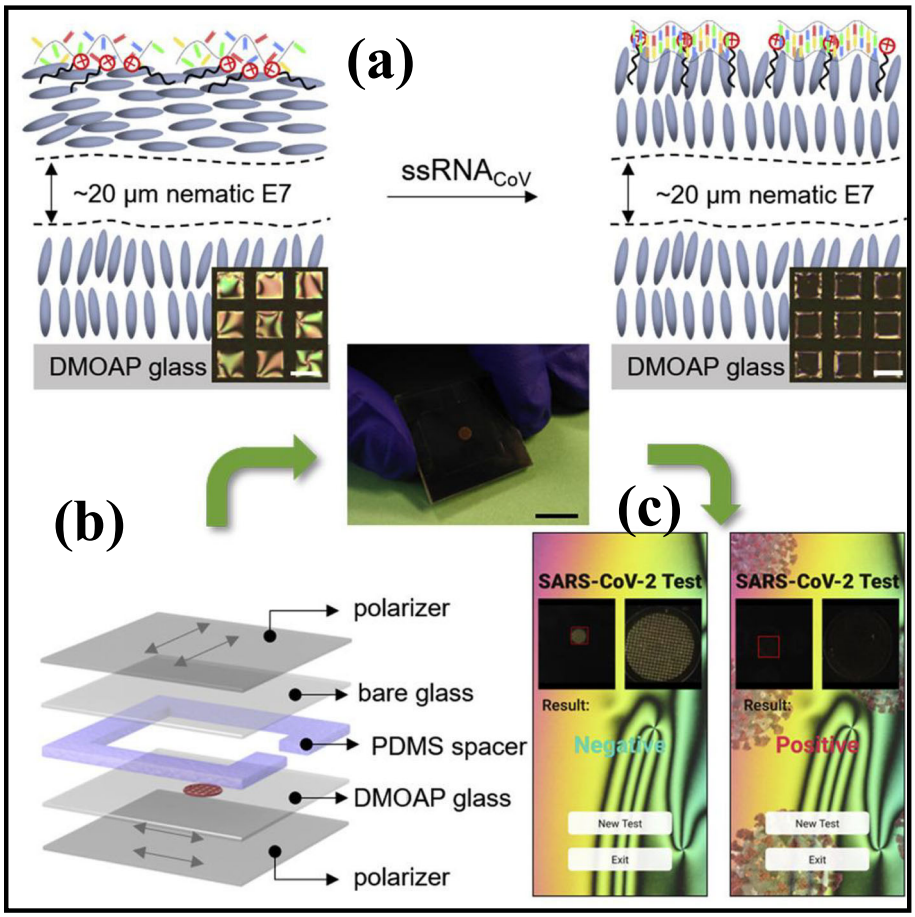

FIGURE 13 (a) Schematic illustration of the optical response of the DTAB/ssDNAprobe-decorated LC film to the adsorption of ssRNASARS test, (b) LC-based naked-eye home detection kit for SARS-CoV-2 and (c) result readout by smartphone app for negative (upon adsorption of < 100 nM $ssRNA_{CoV}$) and positive (upon adsorption of > 30 fM $ssRNA_{CoV}$) test results (adapted from Xu et al.[83] with permission from Cell Press publishing)

found that a concentration of MeTDC greater than 0.1% by weight induced a homeotropic alignment of 5CB molecules producing a dark texture, which turns into a bright one when the sensor was immersed in a water sample containing Hg^{2+} ions. The formation of complex between MeDTC and Hg^{2+} ion caused a small perturbation which changed the orientation of LC molecules leading to change in texture (Figure 14) as observed using POM under crossed polarizers. The sensor showed a good specificity towards Hg^{2+} ions when water samples containing heavy metal ions such as Hg^{2+}, Pb^{2+}, Cd^{2+}, Zn^{2+}, Cu^{2+}, Na^{+}, Ca^{2+} and Mg^{2+} were analysed and showed the change in texture only with Hg^{2+} ions in a wide range of detection from 5 μM to 100 μM with a lowest detection limit of 0.5 μM in deionized water.

In a further development, Hong et al.[88] have reported a LC based droplet based aptasensor for Hg^{2+} ion detection. Aptamer has been designed in such a way that it forms a hairpin structure in the presence of Hg^{2+}. The sensing mechanism is based on the interaction of negatively charged Hg^{2+} specific aptamer and positive charge trimethyl octadecyl ammonium bromide (OTAB) that induces a planer alignment of LC showing a bright fan-shaped pattern under POM. However, in the presence of Hg^{2+}, the electrostatic interaction between OTAB and aptamer is broken down by hairpin structure of aptamer formed upon binding with Hg^{2+} ions, thus rearranges the LC molecules towards homeotropic orientation at the LC–aqueous interface, showing a dark texture with high sensitivity with a LOD of 100 pM Hg^{2+} in buffer sample.

An aptamer based heavy metal ion detector is reported by Verma et al.[89] using 5CB LC for the optical detection of lead (Pb^{2+}) ions in aqueous solution using a novel approach of utilizing spinach RNA. Gold TEM grids placed on DMOAP modified glass slides and filled with 5CB LC showed a bright optical appearance which subsequently changed to dark texture when a cationic surfactant cetyltrimethylammonium bromide (CTAB) of concentration 7 μM was self-assembled on it. The hydrophobic interaction between the hydrocarbons chain of CTAB and 5CB LC induced a change in the alignment of LC from planar/tilted to homeotropic. The addition of negatively charged target recognition probe, spinach RNA aptamer (SRNA) electrostatically interacted with positively charged CTAB layer disrupting the self-assembly at the interface. This disturbance changed the orientation of LC to planar again altering the texture from dark to bright. In presence of Pb^{2+} ions, SRNA forms a G-quadruplex complex with the Pb^{2+} ion leading to a conformational change in the aptamer that destabilizes the CTAB–SRNA interaction at the interface. This again encouraged the hydrophobic coupling between CTAB and 5CB molecules regenerating the homeotropic transitions of LC (bright to dark). The SRNA based LC sensor has been found to detect Pb^{2+} in water samples in a wide detection range from 3 to 300 nM with a LOD of 3 nM. The specificity of the sensor was checked in the presence of other heavy metal ions such as Co^{2+}, Hg^{2+}, Ni^{2+}, and Zn^{2+} which did not show any optical change within observational time of 20 min while an alteration in brightness was observed within 5–10 min. in the case of Pb^{2+} ions. In a similar approach, Nguyen and Jang[90] developed a sensor for the detection of arsenic (As^{3+}) ions in water using a 100-mer DNA aptamer specific for arsenic binding (Ars-3) as a molecular recognition element. Ars-3 aptamers specifically binds to As^{3+}

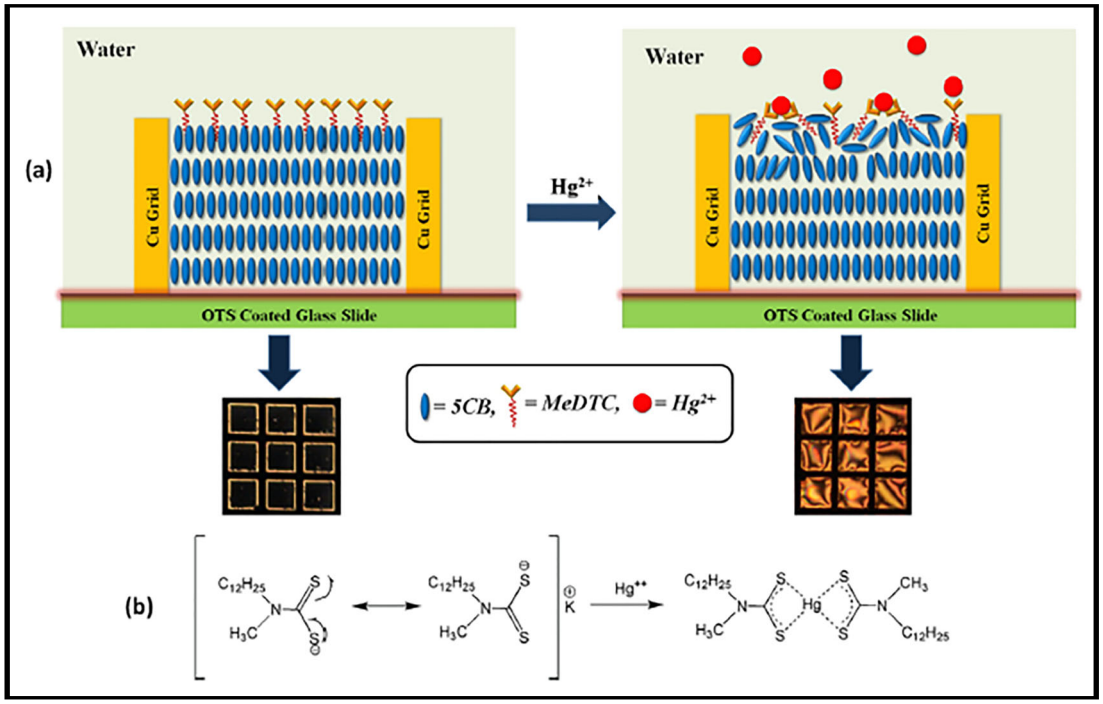

FIGURE 14 (a) Schematic illustration of orientational transitions of 5CB molecules doped with MeDTC at LC–aqueous interface in the absence and presence of Hg^{2+} ions and (b) resonance hybrid structures of MeDTC and Hg-MeDTC (adapted from Singh et al.[87] with permission from Elsevier)

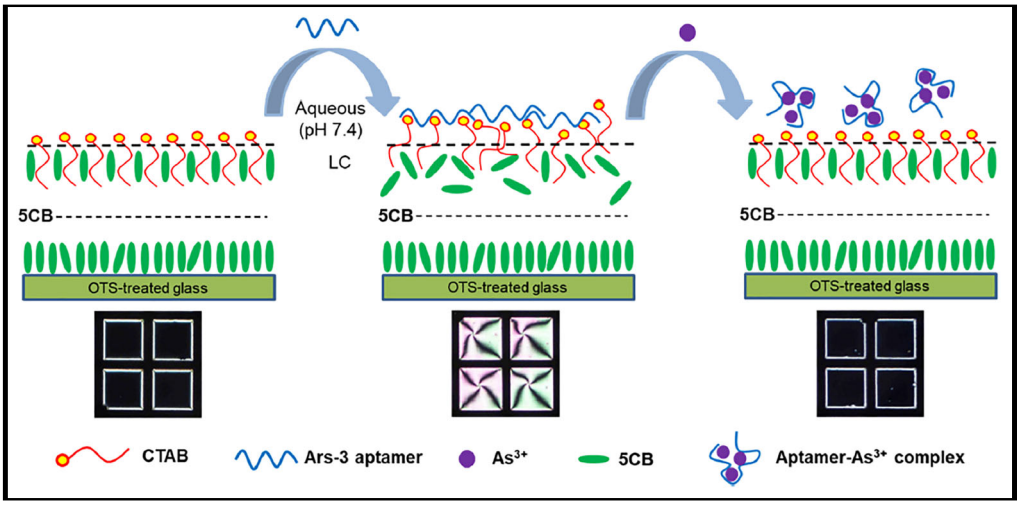

FIGURE 15 Schematic illustration of the LC-based biosensor for the detection of As^{3+} ions based on the self-assembly of CTAB at the interface, influenced by a conformational change of the Ars-3 aptamer upon binding with the target. The lower images represent the polarized optical micrographs corresponding to the respective interfacial events at the aqueous–LC interface (adapted from Nguyen and Jang[90] with permission from Elsevier)

ions in aqueous solution to form a complex (Figure 15) which disrupts the CTAB–(Ars-3) interaction which is reflected in the change in orientation of 5CB molecules observed under POM. The sensing system has a LOD value of 50 nM (~3.7 ppb) and detection range from 50 to 500 nM. The selectivity studies were performed at 500 nM concentration using other potential ions such as Ca^{2+}, Co^{2+}, Hg^{2+}, Ni^{2+}, Fe^{2+}, Pb^{2+}. No significant change in the optical images and their corresponding AGI (average grayscale intensity) has been observed indicating the selectivity of the spinach RNA based probe for specific detection of arsenic in water samples.

LC-doped aggregation-induced emission (AIE) luminogen-based fluorescence is reported by Du et al.[91] for detection of Pb^{2+} ions. This fluorescence sensor is based on a principle of change in LC configuration by DNAzyme strand and its catalytic cleavage in the presence of Pb^{2+} ions leading to a reduction in the fluorescence intensity. The fluorescence sensor is capable of detecting Pb^{2+} over a concentration range of 20 nM to 100 μM with a LOD of 0.65 nM, which is lower by two orders of magnitude than the earlier reported LOD of 36.8 nM obtained from LC-based Pb^{2+} optical sensor.[119]

3.4 | Detection of environmental organic pollutants

Sensing technologies for the detection of organic pollutants are attaining a lot of interest due to their importance in environment monitoring. However, the existing current technologies are expensive and complex, which limit the useful range of real-time application. In this context, LC-based optical sensors for detecting environmental pollutants are attaining a lot of interest owing to their simplicity.[92–94,120] Enzyme inhibited pesticides such as baycarb, dimethoate, fenobucarb and malathion, are toxic to humans, animals and aquatic lives as they inhibit the enzyme activity of AChE causing many eco-toxicological problems. Malathion (MA) is also considered an environmental contaminant with high toxicity and carcinogenicity, possessing serious public health problems. Cationic surfactant, Myr, induces either homeotropic (on an open silane treated glass plate/copper grid) or planar (in enclosed cell) alignment of LC at aqueous–LC interface, which becomes perturbed by AchE due to enzymatic hydrolysis of Myr. However, the enzymatic hydrolysis of Myr in the presence of AChE is inhibited by enzyme inhibitors such as organophosphate or carbamate based pesticides, which assists LCs to reorient them to their original alignment, exhibiting optical response with increasing concentration of pesticides. Wang et al. have developed a sensitive LC-droplet platform using AChE with cationic surfactant, Myr for the sensitive detection of baycarb and dimethoate with a detection limit of 1.0 ng ml^{-1} and 0.1 ng ml^{-1}, respectively.[92] Qi et al.[93] have utilized supramolecular spheres made of poly(oxometallate) and sodium dodeca tungsto phosphate (PW_{12}) with Myr, for the detection of dimethoate pesticide in the presence of AChE at the LC–aqueous interface. The LC optical response detected the dimethoate concentration up to lowest concentration of 0.9 ng ml^{-1}. However, these LC-droplet platforms prepared on OTS-treated glass plate/copper grid have disadvantages of high sample volume requirement and low stability of A few minutes, at room temperature, due to evaporation of solution as LC-aqueous droplets are exposed to open environment resulting in the exposure to heat, vibration and air flow. These drawbacks have been addressed by Nguyen and Jang[94] by confining the LC-droplet in micro-capillaries for the detection of fenobucarb and MA using principle of AChE inhibition. In OTS treated capillary, the surfactant Myr provides a planar alignment at LC–aqueous interface in contrast to homeotropic alignment obtained in OTS-treated glass plate reported earlier,[93] as the LC-droplet is confined between the OTS-treated surrounding surface in microcapillary, showing a texture of a four-petal shape that upon

reacting with AChE becomes reoriented to original alignment due to Myr hydrolysis by AchE with an optical texture of two-bright lined image (Figure 16(I)). This type of homeotropic alignment induced by AChE is inhibited by enzyme inhibitor pesticide, exhibiting bright four-petal shape with the increasing concentration of fenobucarb (Figure 16(II)) with LOD of 5 pg ml^{-1} and 2.5 pg ml^{-1}. This LOD of 2.5 pg ml^{-1} MA is much lower than that of earlier reported LOD of 0.465 nM (Table 1) by the same group[120] using MA-specific aptameric oligonucleotide sequence having 72 nucleotides [5′ATCCGTCACACCTGCTCTTATACACAATTGTTTT TCTCTTAACTTCTTGACTGCTGGTGTTGGCTCCCGTAT-3′] in conjunction with cationic surfactant, CTAB.

Kim Hong and Jang[95] have also reported a highly sensitive LC-aptamer sensor for MA with a LOD of 2.5 pM (0.826 pg ml^{-1}) by using MA-specific 72-mer aptamers (5′-ATCCGTCACACCTGCTCT TATACACAATTGTTTTTCTCTTAACTTCTTGACTGCTGGTGTTGGCT-CCCGTAT-3′) covalently immobilized on (3-glycidyloxypropyl) trimethoxysilane (GOPS)/DMOAP self-assembled monolayer modified glass slides. The interaction of MA with immobilized aptamers leads to a change in orientation of LC from homeotropic (dark) to planar (bright) under POM. Water and soil samples spiked with MA were also analysed using this sensor. The LOD of 100 pM (~33.036 pg ml^{-1}) and 50 pM (~16.518 pg ml^{-1}) were found in spiked tap water and spiked soil samples, respectively. Zhou et al.[96] have used the enzymatic activity of alkaline phosphatase (ALP) for the detection of dichlorvos (DDVP) pesticide up to the lowest detection limit of 0.1 ng ml^{-1}. Bisphenol A (BPA) is another environmental contaminant which can disrupt endocrine system in humans and induce damages to reproductive function, leads to miscarriages and can cause cancer.[121] Ren et al.[97] have developed a LC for the detection of BPA

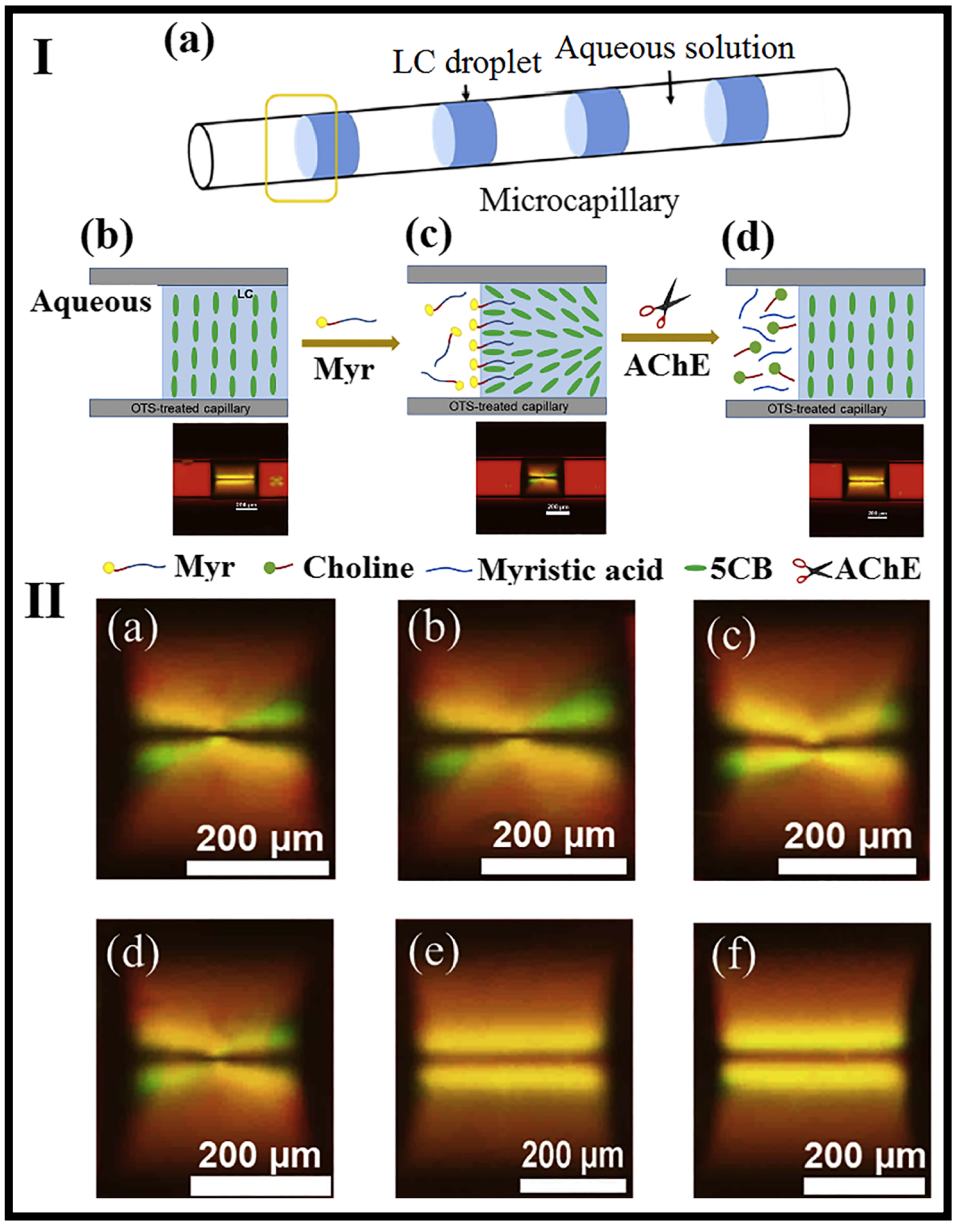

FIGURE 16 Schematic illustration of the LC-based microcapillary sensor. (I) The formation of LC droplets inside an OTS-treated microcapillary (a), the orientation transition of LC molecules generated in (b) pure PBS solution (pH 7.4), (c) Myr aqueous solution, and (d) a mixed solution of Myr and AChE. (II) Polarized optical microscopy images of LC droplets confined in a microcapillary when in contact with a pre-incubated mixture of 30 μM Myr, 2.5 μg ml^{-1} AChE and different concentrations of fenobucarb in river water: (a) 0 pg ml^{-1} (only river water), (b) 1 pg ml^{-1}, (c) 5 pg ml^{-1}, (d) 25 pg ml^{-1}. (adapted from Nguyen and Jang[94] with permission from Elsevier)

using aptamer (5′ amino C6 modified oligo nucleotide aptamer sequence having 60 mers) as binding ligand. A self-assembled monolayer of APTES/DMOAP has been deposited on the glass slides which offer functional groups for the binding of biomolecules on it. The long hydrocarbon chains present on the layer leads to vertical alignment of LC generating a black texture when observed using POM. Further BPA aptamer was covalently immobilized on a glass slide using GA via a stable amide bond between the amino group of 3′-end of aptamer chain and aldehyde group of GA. Immobilization of aptamer on glass surface produced no change in the orientation of LC which remained homeotropic leading to a black texture. On addition of BPA, a complex is formed between the aptamer and BPA causing a change in the conformation of aptamer molecules which disrupt the alignment of LC. This disturbance on the surface of the LC cell leads to a change in orientation of 5CB LC molecules from homeotropic (black) to random (bright). The intensity of brightness was found to increase linearly with the increasing concentration of BPA from 600 pM to 20 nM with a LOD of 600 pM. Polychlorinated biphenyls (PCBs) are highly toxic synthetic organic pollutants and their detection and minimization is very important for global food safety and environmental preservation. A LC- aptamer sensor based on triple-helix molecular switch (THMS) structure has been developed by Verdian et al.[98] for the detection of 3,3′,4,4′-tetrachlorobiphenyl (PCB77). The operating principle of this sensor is based on single transduction probe (5' amino C6 modified CTCTCTCTCTCTCT-3′) in THMS with a PCB77 specific aptamer, which upon reacting with PCB77 breaks down to THMS and the released STP becomes hybridized to complementary STP (5′-AGAGAGAGAGAGAG-3′) immobilized on the cell surface making a configurational change in the LC configuration, resulting to a bright optical appearance corresponding to a PCB77 concentration as low as 1.5×10^{-5} μg L^{-1}.

4 | CONCLUSIONS AND FUTURE PERSPECTIVES

This review article summarizes some of the most recent findings in the field of novel LC-based biosensors for detection of chemical and biological analytes. The unique and exciting feature of LCs to show change in its orientation on exposure to various stimuli provides a myriad of opportunities for the development of novel smart functional materials that holds the promise for major advances in biosensor applications. The research achievements discussed in this review article robustly implies that the approach of the researchers for developing LC-based biosensors is indeed a very promising aspect but still there are many major issues that need to be addressed before these LC-based biosensors could give any competitive challenge to the biological sensors already in the market. Some of the key issues related to these sensors are: (a) sturdiness of LC films on flat surfaces to be used in aqueous solution, (b) requirement of lower LOD values in comparison to existing non-LC-based biosensors, (c) development of true and reliable specific biosensors using antibodies, aptamers and similar biomolecules, (d) reproducibility and long shelf-lives of the pre-fabricated LC-based biosensing devices, (e) detection of specific analytes by LC-based biosensors in the presence of interfering species. These are some of the extremely important issues that need to be extensively researched before any serious attempts are made to commercialize new types of LC-based biosensors. A clear understanding of the phenomena of LC–biomolecules interaction and biomolecular reactions involved at the molecular level in the analyte detection will facilitate in successful development of highly advanced LC-based biosensors. With the increasing amount of researchers continuing their endeavours in research and development of LC materials based biosensors, vast incremental advances and technological leaps are expected in this field in the near future. The study of various biological interactions using LC-interface, as described in this review, can assist in developing cures for various diseases. The development of rapid, portable and inexpensive LC-based diagnostic tools will facilitate in substantially improving the healthcare in developing countries that will enhance their capacity to respond to domestic disasters.

ACKNOWLEDGEMENTS

The authors are grateful to Director, National Physical Laboratory, New Delhi, India for providing the facilities. Lokesh K. Ganwar is thankful to the Council of Scientific and Industrial Research, India for providing a senior research fellowship (SRF).

DECLARATION OF INTEREST STATEMENT

There are no conflicts to declare.

ORCID

Rajesh https://orcid.org/0000-0002-5913-0657

REFERENCES

[1] P. Palffy-Muhoray, *Phys. Today* **2007**, *60*, 54.
[2] Q. Li, in *Liquid Crystals Beyond Displays*, (Ed: Q. Li), John Wiley & Sons, Inc., Hoboken, NJ, USA **2012**.
[3] A. J. Beekman, J. Nissinen, K. Wu, K. Liu, R. J. Slager, Z. Nussinov, V. Cvetkovic, J. Zaanen, *Dual gauge field theory of quantum liquid crystals in two dimensions*, Elsevier B.V. **2017**.
[4] A. J. Beekman, J. Nissinen, K. Wu, J. Zaanen, *Phys. Rev. B* **2017**, *96*, 165115.
[5] G. A. Di Lisi, J. J. De Luca, in *An introduction to liquid crystals*, (Ed: J. J. DeLuca), Morgan & Claypool Publishers **2019**.
[6] P. G. de Gennes, J. Prost, *The Physics of Liquid Crystals*, Clarendon Press **1993**.
[7] P. J. Collings, M. Hird, *Introduction to Liquid Crystals Chemistry and Physics*, 1st ed., Taylor & Francis, Abingdon, UK **1997**.
[8] J. D. Parsons, *Phys. Rev. A* **1979**, *19*, 1225.
[9] H. Kawamoto, *Proc. IEEE* **2002**, *90*, 460.
[10] C. Luan, H. Luan, D. Luo, *Micromachines* **2020**, *11*, 176.
[11] Z. Wang, T. Xu, A. Noel, Y.-C. Chen, T. Liu, *Soft Matter* **2021**, *17*, 4675.
[12] Z. Khoshbin, K. Abnous, S. M. Taghdisi, A. Verdian, *TrAC Trends Anal. Chem.* **2021**, *142*, 116325.
[13] S. Liao, Y. Qiao, W. Han, Z. Xie, Z. Wu, G. Shen, R. Yu, *Anal. Chem.* **2012**, *84*, 45.
[14] H. Tan, S. Yang, G. Shen, R. Yu, Z. Wu, *Angew. Chem. Int. Ed. Engl.* **2010**, *49*, 8608.

[15] S. V. Shiyanovskii, T. Schneider, I. I. Smalyukh, T. Ishikawa, G. D. Niehaus, K. J. Doane, C. J. Woolverton, O. D. Lavrentovich, *Phys. Rev. E* **2005**, *71*, 020702.
[16] S.-W. Tam-Chang, L. Huang, *Chem. Commun.* **2008**, 1957.
[17] J. Fang, U. Gehlert, R. Shashidar, C. M. Knobler, *Langmuir* **1999**, *15*, 297.
[18] P. Popov, E. K. Mann, A. Jákli, *Phys. Rev. Appl.* **2014**, *1*, 034003.
[19] W. Iglesias, N. L. Abbott, E. K. Mann, A. Jákli, *ACS Appl. Mater. Interfaces* **2012**, *4*, 6884.
[20] R. J. Carlton, J. T. Hunter, D. S. Miller, R. Abbasi, P. C. Mushenheim, L. N. Tan, N. L. Abbott, *Liq. Cryst. Rev.* **2013**, *1*, 29.
[21] L. N. Tan, R. Carlton, K. Cleaver, N. L. Abbott, *Mol. Cryst. Liq. Cryst.* **2014**, *594*, 42.
[22] P. Popov, E. K. Mann, A. Jákli, *J. Mater. Chem. B* **2017**, *5*, 5061.
[23] J. T. Hunter, N. L. Abbott, *Sens. Actuators B* **2013**, *183*, 71.
[24] C. G. Reyes, A. Sharma, J. P. F. Lagerwall, *Liq. Cryst.* **1986**, *2016*, 43.
[25] P. V. Shibaev, M. Wenzlick, J. Murray, A. Tantillo, J. Howard-Jennings, *Adv. Condens. Matter Phys.* **2015**, *2015*, 1.
[26] A. Hussain, A. T. S. Semeano, S. I. C. J. Palma, A. S. Pina, J. Almeida, B. F. Medrado, A. C. C. S. Pádua, A. L. Carvalho, M. Dionísio, R. W. C. Li, H. Gamboa, R. V. Ulijn, J. Gruber, A. C. A. Roque, *Adv. Funct. Mater.* **2017**, *27*, 1700803.
[27] P. Popov, L. W. Honaker, E. E. Kooijman, E. K. Mann, A. I. Jákli, *Sens. Bio-Sensing Res.* **2016**, *8*, 31.
[28] V. K. Gupta, J. J. Skaife, T. B. Dubrovsky, N. L. Abbott, *Science* **1998**, *279*, 2077.
[29] J. M. Brake, N. L. Abbott, *Langmuir* **2007**, *23*, 8497.
[30] S. V. Shiyanovskii, O. D. Lavrentovich, T. Schneider, T. Ishikawa, I. I. Smalyukh, C. J. Woolverton, G. D. Niehaus, K. J. Doane, *Mol. Cryst. Liq. Cryst.* **2005**, *434*, 259.
[31] S. J. Woltman, G. D. Jay, G. P. Crawford, *Nat. Mater.* **2007**, *6*, 929.
[32] X. Bi, S. Huang, D. Hartono, K.-L. Yang, *Sens. Actuators B* **2007**, *127*, 406.
[33] C.-Y. Xue, K.-L. Yang, *Langmuir* **2008**, *24*, 563.
[34] S.-H. Sun, M.-J. Lee, Y.-H. Lee, W. Lee, X. Song, C.-Y. Chen, *Biomed. Opt. Express* **2015**, *6*, 245.
[35] H.-W. Su, Y.-H. Lee, M.-J. Lee, Y.-C. Hsu, W. Lee, *J. Biomed. Opt.* **2014**, *19*, 077006.
[36] H.-W. Su, M.-J. Lee, W. Lee, *J. Biomed. Opt.* **2015**, *20*, 057004.
[37] S.-R. Kim, N. L. Abbott, *Adv. Mater.* **2001**, *13*, 1445.
[38] J. M. Brake, A. D. Mezera, N. L. Abbott, *Langmuir* **2003**, *19*, 6436.
[39] N. A. Lockwood, J. J. de Pablo, N. L. Abbott, *Langmuir* **2005**, *21*, 6805.
[40] M. Khan, S.-Y. Park, *Sens. Actuators B* **2014**, *202*, 516.
[41] H. J. Kim, J. Rim, C.-H. Jang, *ACS Appl. Mater. Interfaces* **2017**, *9*, 21209.
[42] M. Zhang, C.-H. Jang, *Anal. Biochem.* **2014**, *455*, 13.
[43] J. K. Gupta, S. Sivakumar, F. Caruso, N. L. Abbott, *Angew. Chem. Int. Ed.* **2009**, *48*, 1652.
[44] W. Zhang, W. T. Ang, C.-Y. Xue, K.-L. Yang, *ACS Appl. Mater. Interfaces* **2011**, *3*, 3496.
[45] J. Kim, M. Khan, S.-Y. Park, *ACS Appl. Mater. Interfaces* **2013**, *5*, 13135.
[46] Y.-D. Jung, M. Khan, S.-Y. Park, *J. Mater. Chem. B* **2014**, *2*, 4922.
[47] M. Zhang, C.-H. Jang, *ChemPhysChem* **2014**, *15*, 2569.
[48] T. Bera, J. Deng, J. Fang, *J. Phys. Chem. B* **2014**, *118*, 4970.
[49] S. Sivakumar, K. L. Wark, J. K. Gupta, N. L. Abbott, F. Caruso, *Adv. Funct. Mater.* **2009**, *19*, 2260.
[50] Q.-Z. Hu, C.-H. Jang, *Liq. Cryst.* **2011**, *38*, 1209.
[51] Z. An, Y. Wei, C.-H. Jang, *Liq. Cryst.* **2016**, *44*, 1.
[52] S. Setia, S. Sidiq, J. De, I. Pani, S. K. Pal, *Liq. Cryst.* **2016**, *43*, 2009.
[53] J. J. Skaife, N. L. Abbott, *Langmuir* **2000**, *16*, 3529.
[54] N. L. A. N. A. Lockwood, K. D. Cadwell, F. Caruso, *Adv. Mater.* **2006**, *18*, 850.
[55] M. I. Kinsinger, B. Sun, N. L. Abbott, D. M. Lynn, *Adv. Mater.* **2007**, *19*, 4208.
[56] Rajesh, K. Kumar, S. K. Mishra, P. Dwivedi, G. Sumana, TrAC Trends Anal. Chem. **2019**, *118*, 666.
[57] Rajesh, Z. Gao, R. Vishnubhotla, P. Ducos, M. D. Serrano, J. Ping, M. K. Robinson, A. T. C. Johnson, Adv. Mater. Interfaces **2016**, *3*, 1600124.
[58] H. Bhardwaj, C. A. Marquette, P. Dutta, Rajesh, G. Sumana, *Anal. Bioanal. Chem.* **2020**, *412*, 7029.
[59] S. Singh, A. Kumar, S. Khare, A. Mulchandani, Rajesh, *Appl. Phys. Lett.* **2014**, *105*, 213701.
[60] H. Bhardwaj, M. K. Pandey, Rajesh, G. Sumana, *Microchim. Acta* **2019**, *186*, 592.
[61] Rajesh, Z. Gao, A. T. C. Johnson, N. Puri, A. Mulchandani, D. K. Aswal, *Appl. Phys. Rev.* **2021**, *8*, 011311.
[62] B. Leca-Bouvier, L. J. Blum, *Anal. Lett.* **2005**, *38*, 1491.
[63] A. Warsinke, *Anal. Bioanal. Chem.* **2009**, *393*, 1393.
[64] A. D. Price, D. K. Schwartz, *J. Am. Chem. Soc.* **2008**, *130*, 8188.
[65] S. L. Lai, S. Huang, X. Bi, K.-L. Yang, *Langmuir* **2009**, *25*, 311.
[66] C.-H. Chen, K.-L. Yang, *Langmuir* **2010**, *26*, 1427.
[67] Y. Liu, K.-L. Yang, *J. Colloid Interface Sci.* **2015**, *439*, 149.
[68] S. Yang, Y. Liu, H. Tan, C. Wu, Z. Wu, G. Shen, R. Yu, *Chem. Commun.* **2012**, *48*, 2861.
[69] I. Verma, S. Sidiq, S. K. Pal, *ACS Omega* **2017**, *2*, 7936.
[70] C.-Y. Xue, S. A. Khan, K.-L. Yang, *Adv. Mater.* **2009**, *21*, 198.
[71] E. Zapp, E. Westphal, H. Gallardo, B. de Souza, I. Cruz Vieira, *Biosens. Bioelectron.* **2014**, *59*, 127.
[72] K. Lee, K. C. Gupta, S.-Y. Park, I.-K. Kang, *J. Mater. Chem. B* **2016**, *4*, 704.
[73] T. Govindaraju, P. J. Bertics, R. T. Raines, N. L. Abbott, *J. Am. Chem. Soc.* **2007**, *129*, 11223.
[74] A. M. Lowe, B. H. Ozer, Y. Bai, P. J. Bertics, N. L. Abbott, *ACS Appl. Mater. Interfaces* **2010**, *2*, 722.
[75] V. Sharma, A. Kumar, P. Ganguly, A. M. Biradar, *Appl. Phys. Lett.* **2014**, *104*, 043705.
[76] C.-H. Lin, M.-J. Lee, W. Lee, *Appl. Phys. Lett.* **2016**, *109*, 093703.
[77] P.-C. Wu, A. Karn, M.-J. Lee, W. Lee, C.-Y. Chen, *Dyes Pigm.* **2018**, *150*, 73.
[78] C.-M. Lin, P.-C. Wu, M.-J. Lee, W. Lee, *Sens. Actuators B* **2019**, *282*, 158.
[79] E.-Y. Chuang, P.-Y. Lin, P.-F. Wang, T.-R. Kuo, C.-H. Chen, Y. B. Manga, Y.-C. Hsiao, *Int. J. Nanomedicine* **2021**, *16*, 763.
[80] X. Su, W. Huo, D. Yang, C. Luan, J. Xu, *Talanta* **2019**, *203*, 203.
[81] M. Tyagi, A. Chandran, T. Joshi, J. Prakash, V. V. Agrawal, A. M. Biradar, *Appl. Phys. Lett.* **2014**, *104*, 154104.
[82] Y. Wang, Q. Hu, Y. Guo, L. Yu, *Biosens. Bioelectron.* **2015**, *72*, 25.
[83] Y. Xu, A. M. Rather, S. Song, J.-C. Fang, R. L. Dupont, U. I. Kara, Y. Chang, J. A. Paulson, R. Qin, X. Bao, X. Wang, *Cell Reports Phys. Sci.* **2020**, *1*, 100276.
[84] D. Nguyen, C.-H. Jang, *Micromachines* **2021**, *12*, 370.
[85] C. Xia, D. Zhou, Y. Su, G. Zhou, L. Yao, W. Sun, Y. Liu, *Analyst* **2020**, *145*, 4569.
[86] S. Yang, C. Wu, H. Tan, Y. Wu, S. Liao, Z. Wu, G. Shen, R. Yu, *Anal. Chem.* **2013**, *85*, 14.
[87] S. K. Singh, R. Nandi, K. Mishra, H. K. Singh, R. K. Singh, B. Singh, *Sens. Actuators B* **2016**, *226*, 381.
[88] P. T. K. Hong, K. Yun, C.-H. Jang, *Biochip J.* **2021**, *15*, 152.
[89] I. Verma, M. Devi, D. Sharma, R. Nandi, S. K. Pal, *Langmuir* **2019**, *35*, 7816.
[90] D. K. Nguyen, C.-H. Jang, *Microchem. J.* **2020**, *156*, 104834.
[91] X. Du, Y. Liu, F. Wang, D. Zhao, H. F. Gleeson, D. Luo, *ACS Appl. Mater. Interfaces* **2021**, *13*, 22361.
[92] Y. Wang, Q. Hu, T. Tian, L. Yu, *Sens. Actuators B* **2017**, *238*, 676.
[93] L. Qi, W. Wu, Q. Kang, Q. Hu, L. Yu, *Food Chem.* **2020**, *320*, 126683.

[94] D. K. Nguyen, C.-H. Jang, *Colloids Surf. B Biointerfaces* **2021**, *200*, 111587.
[95] P. T. Kim Hong, C.-H. Jang, *Anal. Biochem.* **2020**, *593*, 113589.
[96] L. Zhou, Q. Hu, Q. Kang, L. Yu, *Talanta* **2018**, *190*, 375.
[97] H. Ren, Z. An, C.-H. Jang, *Microchem. J.* **2019**, *146*, 1064.
[98] A. Verdian, Z. Rouhbakhsh, E. Fooladi, *J. Hazard. Mater.* **2021**, *402*, 123531.
[99] J. Hoogboom, K. Velonia, T. Rasing, A. E. Rowan, R. J. M. Nolte, *Chem. Commun.* **2006**, 434.
[100] A. Niemz, T. M. Ferguson, D. S. Boyle, *Trends Biotechnol.* **2011**, *29*, 240.
[101] J. Kirby, P. R. Heath, P. J. Shaw, *F. C. Hamdy* **2007**, 247.
[102] D. Prasad, A. S. Vidyarthi, *Afr. J. Biotechnol.* **2009**, *8*, 1768.
[103] M. N. Velasco-Garcia, T. Mottram, *Biosyst. Eng.* **2003**, *84*, 1.
[104] H.-R. Kim, J.-H. Kim, T.-S. Kim, S.-W. Oh, E.-Y. Choi, *Appl. Phys. Lett.* **2005**, *87*, 143901.
[105] M. Nakata, G. Zanchetta, M. Buscaglia, T. Bellini, N. A. Clark, *Langmuir* **2008**, *24*, 10390.
[106] S. M. Malone, D. K. Schwartz, *Langmuir* **2011**, *27*, 11767.
[107] J. Prakash, S. Khan, S. Chauhan, A. M. Biradar, *J. Mol. Liq.* **2020**, *297*, 112052.
[108] Y.-Y. Luk, C.-H. Jang, L.-L. Cheng, B. A. Israel, N. L. Abbott, *Chem. Mater.* **2005**, *17*, 4774.
[109] Y.-Y. Luk, M. L. Tingey, K. A. Dickson, R. T. Raines, N. L. Abbott, *J. Am. Chem. Soc.* **2004**, *126*, 9024.
[110] B. H. Clare, N. L. Abbott, *Langmuir* **2005**, *21*, 6451.
[111] P. Kalita, S. S. Shukla, R. K. Singh, A. Bhattacharjee, *Spectrochim. Acta Part A Mol. Biomol. Spectrosc.* **2021**, *254*, 119634.
[112] L. A. Tercero Espinoza, K. R. Schumann, Y.-Y. Luk, B. A. Israel, N. L. Abbott, *Langmuir* **2004**, *20*, 2375.
[113] C.-H. Jang, L.-L. Cheng, C. W. Olsen, N. L. Abbott, *Nano Lett.* **2006**, *6*, 1053.
[114] L.-L. Cheng, Y.-Y. Luk, C. J. Murphy, B. A. Israel, N. L. Abbott, *Biomaterials* **2005**, *26*, 7173.
[115] C. J. Woolverton, E. Gustely, L. Li, O. D. Lavrentovich, *Liq. Cryst.* **2005**, *32*, 417.
[116] Y. Wei, C.-H. Jang, *Sens. Actuators B* **2018**, *254*, 72.
[117] R. J. Carlton, J. K. Gupta, C. L. Swift, N. L. Abbott, *Langmuir* **2012**, *28*, 31.
[118] Q.-Z. Hu, C.-H. Jang, *Colloids Surf. B Biointerfaces* **2011**, *88*, 622.
[119] L. T. Chu, H. M. Leung, P. K. Lo, T.-H. Chen, *Sens. Actuators B* **2020**, *306*, 127564.
[120] D. K. Nguyen, C.-H. Jang, *Biosensors* **2021**, *11*, 92.
[121] C. Pivonello, G. Muscogiuri, A. Nardone, F. Garifalos, D. P. Provvisiero, N. Verde, C. de Angelis, A. Conforti, M. Piscopo, R. S. Auriemma, A. Colao, R. Pivonello, *Reprod. Biol. Endocrinol.* **2020**, *18*, 22.

How to cite this article: Rajesh, L. K. Gangwar, S. K. Mishra, A. Choudhary, A. M. Biradar, G. Sumana, *Luminescence* **2022**, 1. https://doi.org/10.1002/bio.4242